Unroofing the Klamaths—Blame it on Siletzia?

Rachel Piotraschke[1], Susan M. Cashman[2], Kevin P. Furlong[1], Peter J.J. Kamp[3], Martin Danišík[3,4], and Ganqing Xu[3]
[1]DEPARTMENT OF GEOSCIENCES, PENNSYLVANIA STATE UNIVERSITY, UNIVERSITY PARK, PENNSYLVANIA 16802, USA
[2]DEPARTMENT OF GEOLOGY, HUMBOLDT STATE UNIVERSITY, ARCATA, CALIFORNIA 95521, USA
[3]SCHOOL OF SCIENCE, UNIVERSITY OF WAIKATO, HAMILTON 2340, NEW ZEALAND
[4]JOHN DE LAETER CENTRE, DEPARTMENT OF APPLIED GEOLOGY, CURTIN UNIVERSITY, GPO BOX U1987, PERTH, WESTERN AUSTRALIA 6845, AUSTRALIA

ABSTRACT

The Klamath Mountains province of northwestern California–southwestern Oregon is an anomalous element in the Cascadia margin; these mountains have the highest average topography, the oldest rocks, and the only identified example of late Cenozoic detachment faulting in the coastal mountains of the Cascadia forearc. Low-temperature thermochronology (apatite fission-track, apatite [U-Th]/He) analyses from the central and southern Klamath Mountains province record two distinct exhumation events—a Cretaceous–Paleocene regional cooling and a southward-migrating locus of rapid cooling/exhumation in the middle Tertiary. This younger event is localized within the geographic extent of the La Grange fault. We infer that this pattern reflects two distinct processes of exhumation: regional surface erosion (older) and migrating localized tectonic exhumation (younger). At the southern limit of this region of rapid cooling, slickenside striations on the exposed La Grange fault surface record southward displacement of the upper plate along a shallowly dipping (~20°) detachment surface. Thermochronologic data constrain average dip of the fault to a few degrees, upper-plate thickness to <~6–8 km, and fault slip rate to <2 mm/yr for a duration of 30 m.y. (ca. 45 Ma to 15 Ma). The fault dip is unusually low compared to that of typical detachment faults; the duration of this extensional event is unusually long compared to other detachment faults; the north-south (margin-parallel) slip direction is roughly perpendicular to that of other Klamath Mountains province faults; and the Eocene to early Miocene timing of extensional faulting does not correlate with recognized tectonic events in northern California. Mid-Tertiary tectonic events in the Oregon Coast Ranges provide a context for understanding the unusual mid-Tertiary tectonism in the Klamath Mountains province. Immediately north of the Klamath Mountains province, early Eocene accretion of a large early Cenozoic igneous province, the Siletz terrane, initiated a westward jump of active subduction. Accretion was followed by late Eocene margin-parallel extension in the Oregon Coast Ranges, recorded by formation of a regional dike swarm. Both the timing of tectonic exhumation and the direction of extension on the La Grange detachment fault suggest that mid-Tertiary tectonism in the southern Klamath Mountains province was likely driven by plate tectonics associated with the accretion of Siletzia and the reestablishment of subduction outboard of the accreted terrane.

LITHOSPHERE; v. 7; no. 4; p. 427–440 | Published online 13 May 2015 doi:10.1130/L418.1

INTRODUCTION

The Klamath Mountain province (Fig. 1) straddles a fundamental transition in the North America plate boundary from subduction along Cascadia to translation along the San Andreas system, and it is both geologically and topographically distinctive. The orogen's Neogene to Holocene tectonic history potentially provides a window into the evolution of the plate boundary as it underwent the transition from a long history of subduction (Farallon, Juan de Fuca) to encroaching translational (Pacific) plate interactions. The Klamath Mountain province presently hosts some of the highest topography along the convergent boundary (Fig. 1A). Maximum and mean elevations in the Klamath Mountains are higher than those elsewhere in the coastal ranges of Cascadia (Kelsey et al., 1994), and the Klamath Mountain province, consisting of Precambrian to Late Cretaceous, primarily oceanic tectonostratigraphic terranes, includes the oldest (Wallin et al., 1995) and among the most structurally complex (cf. Irwin, 1981, 1985) units along the Cascadia margin. The period during which this high topography developed and the relationship between uplift and exhumation of Paleozoic and Mesozoic bedrock remain unclear.

Active deformation in the southernmost Cascadia subduction zone, at the latitude of the Klamath Mountains province, also differs from that of the rest of the Cascadia margin.

Patterns of seismicity, including the spatial and temporal distribution of episodic tremor and slip events (Fig. 1A; Szeliga et al., 2004; Brudzinski and Allen, 2007; Gomberg et al., 2010; K. Creager, January 2015, personal commun.), anticorrelation of tremor and small upper-plate earthquakes (Boyarko and Brudzinski, 2010; Gomberg et al., 2010), and inferred segmentation of Cascadia subduction zone earthquake history (e.g., Wang et al., 2013), all distinguish the southern part of the Cascadia subduction zone.

This study addresses two fundamental questions:

(1) Does the Klamath topographic massif reflect relict (Late Cretaceous–Early Tertiary) topography, or is it a result of young and/or ongoing uplift linked to the modern plate boundary?

(2) Do the distinctive seismologic characteristics of the southernmost Cascadia subduction zone margin reflect the geologic character of the regional forearc (e.g., crust of the Klamath Mountain province), or are they simply a function of the current plate-tectonic setting independent of upper-plate crustal structure?

In this paper, we present new low-temperature thermochronologic data from the central and southeastern Klamath Mountains, use these to constrain the movement history of a regionally significant fault (the La Grange fault), and examine their implications for the Cenozoic tectonic evolution of the Klamath Mountains province. With new thermochronometry data, we test previous interpretations of Cenozoic history of the Klamath region,

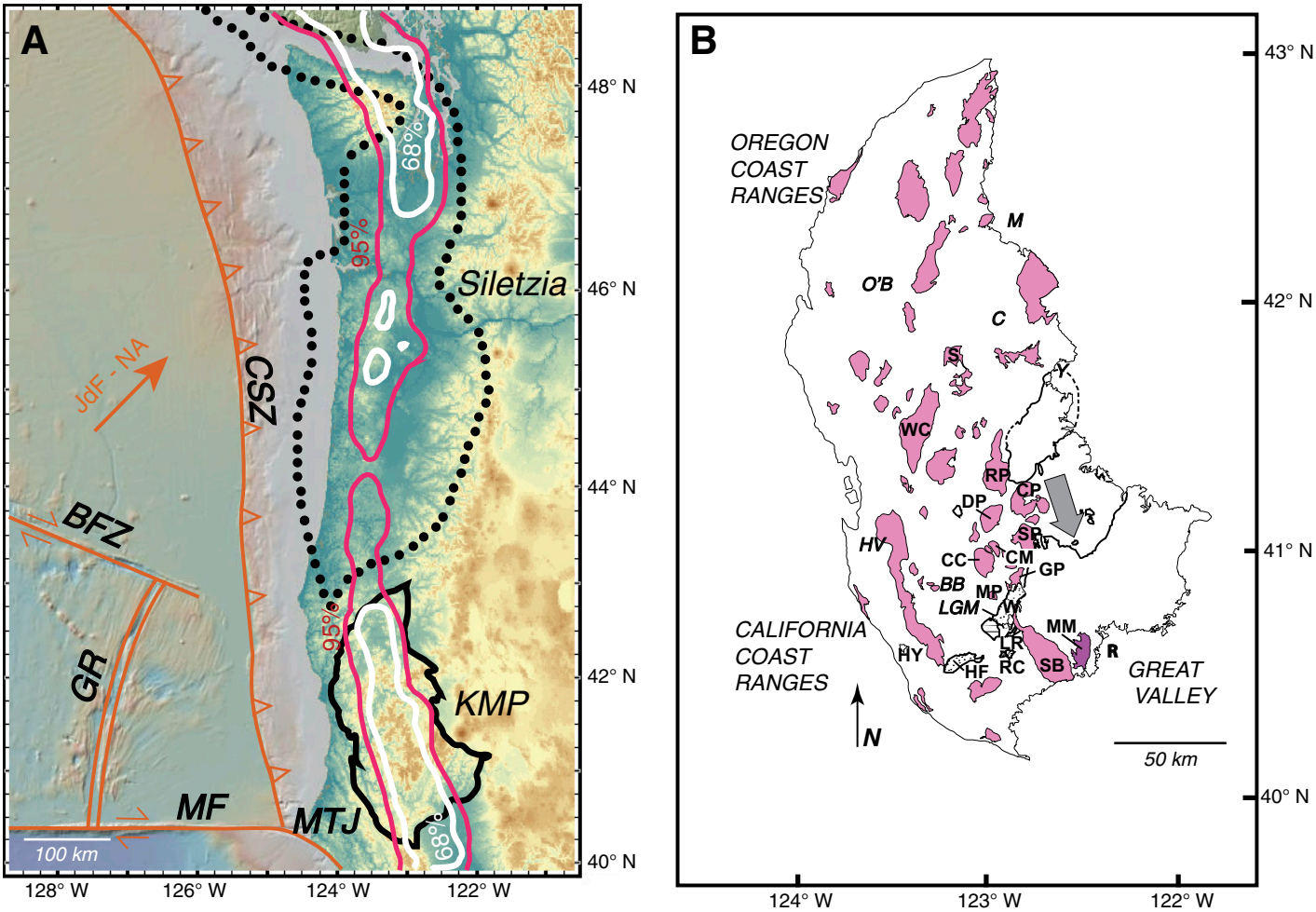

Figure 1. (A) Location map of the Cascadia region showing plate boundaries and geologic provinces. Klamath Mountains province (KMP)—solid black outline; Siletzia—dotted black outline (from Wells et al., 2014); plate boundaries are shown in orange with sense of plate motions indicated: CSZ—Cascadia subduction zone, MF—Mendocino fault, GR—Gorda Ridge, BFZ—Blanco fracture zone, MTJ—Mendocino triple junction; JdF—Juan de Fuca; NA—North America. Contours of seismic tremor (white contours outline regions containing 68% of all tremors, red contours outline regions containing 95% of all tremor activity) are of all tremors between 1 August 2009 and 20 January 2015. This compilation includes all tremors in swarms that lasted more than 5 h. Tremor data are from K. Craeger (2015, personal commun.). Base map is from GeoMapApp. (B) Location map of geologic features in Klamath Mountains province. Bold line—La Grange detachment fault; the large gray arrow shows direction of transport of hanging-wall rocks relative to footwall (measured at La Grange mine, from Cashman and Elder, 2002). Basins containing Tertiary Weaverville Formation are shown with stipple pattern; Jurassic and Cretaceous plutons are shown in pink; Devonian Mule Mountain stock is shown in purple. Locations indicated by italic abbreviations are: BB—Big Bar, C—Condrey Mountain, HV—Hoopa Valley, M—Medford, LGM—La Grange mine, O'B—O'Brien, R—Redding, and Y—Yreka. Plutons and other geologic features are indicated by: CC—Canyon Creek pluton, CM—Caribou Mountain pluton, CP—Craggy Peak pluton, DP—Deadman Peak pluton, GP—Granite Peak pluton, HF—Hayfork basin, HY—Hyampom basin, LR—Lowden Ranch basin, MM—Mule Mountain stock, MP—Monument Peak pluton, RC—Reading Creek basin, RP—Russian Peak pluton, SB—Shasta Bally batholith, S—Slinkard pluton, SP—Sugar Pine pluton, WC—Wooley Creek batholith, W—Weaverville basin.

e.g., Neogene Condrey Mountain dome (Mortimer and Coleman, 1985) and Klamath peneplain (Diller, 1902; Aalto, 2006). We then discuss the spatial and temporal correspondence between mid-Cenozoic tectonic events in the Klamath Mountains province and the accretion of the Siletz terrane in the Oregon Coast Ranges (Wells et al., 2014). We conclude that Cenozoic tectonism in the Klamath Mountains province was linked to events on the Cascadia margin to the north.

Present Setting and Geologic Development

The Klamath Mountain province forms part of the southern forearc margin of the Cascadia subduction zone. The western edge of the Klamath Mountain province lies <120 km east of the Cascadia trench, and its southern tip is approximately at the latitude of the Mendocino triple junction, which marks the present-day transition from subduction to translation along the western margin of North America (Fig. 1A). The Klamath Mountain province lies inboard of the expected swath of primary Mendocino triple junction migration effects (Furlong and Govers, 1999; Furlong et al., 2003; Furlong and Schwartz, 2004; Lock et al., 2006), but if its uplift and exhumation are geologically recent (i.e., since ca. 5 Ma), then Mendocino triple junction tectonics may have played an important role in producing the present-day seismogenic behavior of the province. Crustal thickness within the

Klamath Mountain province is not well constrained, but estimates place it in the 35–40 km range (Zucca et al., 1986; Beaudoin et al., 1996; Liu et al., 2012).

Cretaceous marine to nonmarine sedimentary rocks are deposited on the southern and eastern margins of the province and in isolated patches overlying Klamath Mountain province basement (Sliter et al., 1984; Irwin, 1994; Surpless and Beverly, 2013); these units provide a record of burial depth at the locations where they are preserved. Vitrinite reflectance values of 0.68% VR_0 for Lower Cretaceous coal at Big Bar, California, in the southwestern Klamath Mountain province record a maximum burial depth of ~3.5–4 km (Piotraschke, 2012), whereas 0.79% and 0.83% VR_0 values for Cretaceous organic-rich siltstone at O'Brien, Oregon, in the northwestern Klamath Mountain province record a maximum burial depth of ~5 km (Batt et al., 2010a).

The Klamath Mountains province is bounded by regional-scale thrust faults on the north and west. On the west, Klamath Mountain province rocks are thrust over Cretaceous and younger rocks of the Franciscan complex (Wagner and Saucedo, 1987; McLaughlin et al., 2000). Faulting occurred during the Early Cretaceous or later (McLaughlin et al., 2000). At the northern margin of the Klamath Mountain province, the Siletz River volcanics (Siletzia) were faulted beneath, and perhaps locally over, older Mesozoic terranes, including the westernmost Klamath Mountain province (Wells et al., 2000; DuRoss et al., 2002). Time of initiation of this faulting is unknown, but accretion of Siletzia was complete by 50.5–49 Ma, with folding and thrust faulting continuing locally within Siletzia until deposition of the Tyee Formation at 49–48 Ma (Wells et al., 2014). Approximately 8 m.y. after accretion of Siletzia, the Tillamook magmatic episode marked renewed magmatism within Siletzia, extending from central Oregon to southeastern Washington. This event included basalt-rhyolite magmatism, normal faulting, and formation of regional dike swarms in the forearc. The Tillamook magmatic episode records regional margin-parallel extension between 42 and 34 Ma (Wells et al., 2014).

The Klamath Mountain province consists of a stack of thin, generally eastward-dipping and westward-younging tectonostratigraphic terranes bounded by shallowly east-dipping thrust faults and intruded by multiple belts of plutons (Irwin, 1960, 1972, 1985; Allen and Barnes, 2006). The repeated underthrusting and accretion of these oceanic-derived rocks to form the Klamath Mountain province record sequential westward growth of the North American plate by episodic terrane accretion from earliest Paleozoic through Late Jurassic time (Coney et al., 1980; Irwin and Wooden, 1989; Snoke and Barnes, 2006; Ernst et al., 2008). The intruding Klamath Mountain province plutons range from Paleozoic to Mesozoic in age, with Jurassic and Cretaceous plutons being most common, and they consist primarily of calcic and calc-alkalic rocks (Hotz, 1971; Irwin, 1985; Allen and Barnes, 2006). Many Klamath plutons truncate terrane-bounding thrust faults and thus constrain the timing of these regional thrust faulting events (Irwin, 1985; Hacker et al., 1995; Allen and Barnes, 2006). Detailed petrographic, geochemical, and geochronologic studies have identified at least seven compositionally, temporally, and petrogenetically distinctive plutonic belts (Allen and Barnes, 2006). Of particular interest to this study are the 167–156 Ma Wooley Creek suite, which includes the Russian Peak, Wooley Creek, and Slinkard plutons (Allen and Barnes, 2006; Barnes et al., 1986; Cotkin and Medaris, 1993), the 139–136 Ma granodiorite suite that contains the Shasta Bally pluton (Allen and Barnes, 2006), and the 142–136 Ma tonalite-trondhjemite-granodiorite suite, which encompasses the other plutons in the study area (Fig. 1B; Barnes et al., 1996; Allen and Barnes, 2006). One pre-Mesozoic pluton, the Devonian Mule Mountain stock (Albers et al., 1981), was also analyzed in this study.

Geochemical and petrologic studies of plutons provide estimates of emplacement pressure and temperature, which place limits on subsequent uplift and exhumation. Crystallization of the trondhjemitic Caribou Mountain pluton (a "tonalite-trondhjemite-granodiorite" suite pluton) began at depths of at least 12 km (Barnes et al., 1992), generating hornblende-hornfels facies contact metamorphism of wall rocks (Davis, 1963; Goodge, 1989; Barnes et al., 1992). Geobarometry and thermometry studies for the Jurassic Russian Peak plutonic complex indicate an intrusion pressure of ~300 MPa (~11–12 km) and intrusion temperatures of 900–1000 °C (Cotkin and Medaris, 1993). Mineral assemblages in the contact metamorphic aureole of the Wooley Creek pluton vary considerably from south to north, suggesting estimated pressures from ~300 ± 150 MPa (~11 ± 5 km) at the southern margin to ~650 ± 150 MPa (~25 ± 5 km) at the northeastern contact (Barnes et al., 1986; Coint et al., 2013). In general, studies indicate that the initial emplacement depth of exposed central Klamath Mountain province plutons was ~10–12 km.

A regional-scale Tertiary detachment fault, the La Grange fault, cuts Mesozoic and older rocks in the southern Klamath Mountains (Figs. 1B and 2; Schweickert and Irwin, 1989; Cashman and Elder, 2002). The La Grange fault differs dramatically from older structures because it accommodates margin-parallel extension. The dome-like "Trinity arch" (Irwin and Lipman, 1962) of Trinity terrane ultramafic rocks occupies the La Grange fault footwall (Schweickert and Irwin, 1989). Shallowly SSE- to SSW-plunging slickenside striations at four widely separated locations around the margins of the Trinity arch record north-south displacement on the fault (Cashman and Elder, 2002). Distinctive units such as the Moffett Creek Formation, a calcareous siltstone that contains abundant detrital sericite grains and authigenic calcite rhombs, crop out both in the hanging wall of the fault at the La Grange mine and in the Yreka area, 50 km NNE of the mine (Cashman and Elder, 2002). These units demonstrate a link between upper-plate rocks in these areas and imply a minimum north-south (upper plate to south) displacement of 50–60 km on the La Grange detachment (Cashman and Elder, 2002).

The surface of the La Grange fault, exposed at the La Grange mine, records a prolonged, brittle fault history (Fig. 2) Hydraulic mining of mid-Tertiary auriferous gravels (Weaverville Formation) created a 1-km-long exposure of the shallowly south-dipping fault surface. The normal-fault displacement of the La Grange fault places mid-Paleozoic sedimentary rocks and Tertiary Weaverville Formation over Devonian amphibolite (part of the basement rocks that host younger plutons; Schweickert and Irwin, 1989). Weaverville Formation sediments are dated as early to early middle Miocene based on pollen flora (Barnett, 1989), and they dip shallowly toward the exposed La Grange fault surface at the La Grange mine (MacDonald, 1910; Schweickert and Irwin, 1989). The fault surface is capped by a 25-cm-thick layer of strongly foliated, black cataclasite and ultracataclasite (Cashman and Elder, 2002; Cashman and Cashman, 2006). Parallel downdip slickenside striations on the ultracataclasite layers, slickenside-perpendicular veins, and clasts of both ultracataclasite and vein material in cataclasite layers attest to prolonged brittle extensional transport of hanging-wall rocks (Cashman and Cashman, 2006).

Horizontal displacement on the La Grange fault was not accompanied by substantial vertical displacement in the upper plate. Facies distribution in the Weaverville Formation indicates that these fluviolacustrine sediments were deposited synchronously with displacement on the La Grange fault in several small NE-SW–trending grabens (Barnett, 1989; Phillips and Aalto, 1989). Present stratigraphic thickness of the Weaverville Formation is 360 m in the Weaverville basin (Phillips and Aalto, 1989), and ~335 m in the Reading Creek basin (Barnett, 1989). Vitrinite reflectance values for lig-

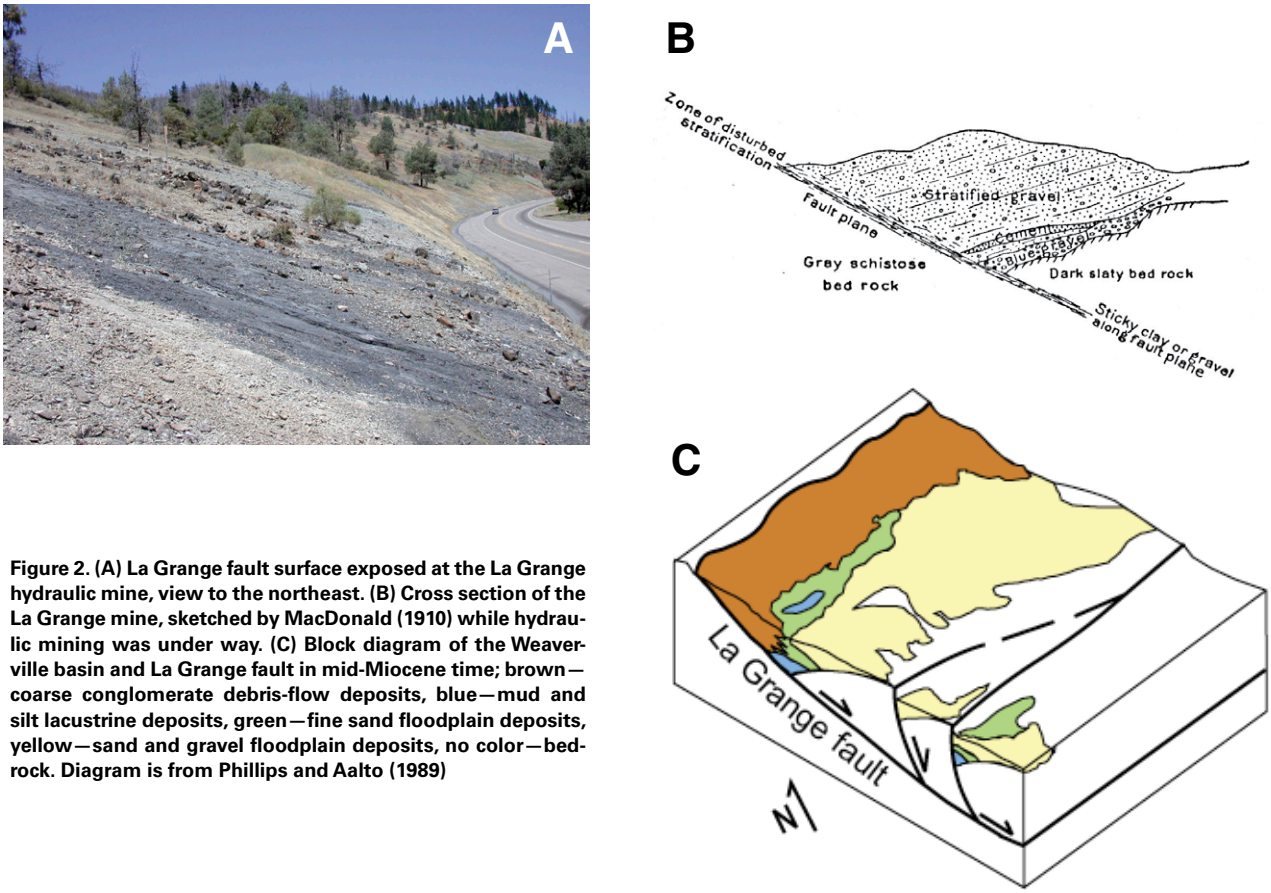

Figure 2. (A) La Grange fault surface exposed at the La Grange hydraulic mine, view to the northeast. (B) Cross section of the La Grange mine, sketched by MacDonald (1910) while hydraulic mining was under way. (C) Block diagram of the Weaverville basin and La Grange fault in mid-Miocene time; brown—coarse conglomerate debris-flow deposits, blue—mud and silt lacustrine deposits, green—fine sand floodplain deposits, yellow—sand and gravel floodplain deposits, no color—bedrock. Diagram is from Phillips and Aalto (1989)

nite sampled from the base of the Weaverville Formation in the Reading Creek basin indicate no significant reheating/burial of these sediments (Piotraschke, 2012).

Timing of Exhumation of the Klamath Mountain Province

Taken together, the geologic characteristics described here reveal a distinctive history for the La Grange fault: prolonged, margin-parallel, extensional faulting at shallow crustal levels, which developed perpendicular to strike of Klamath Mountain province bedrock units. Although the extensional faulting did not result in substantial vertical displacement of rocks in the hanging wall (evidence presented in previous section), it did play a major role in exhuming rocks in the La Grange fault footwall (Batt et al., 2010b). Understanding the timing and duration of slip on the La Grange fault, compared to timing of exhumation of bedrock in other parts of the Klamath Mountains province, is a key to determining the mechanism(s) that drove this extension.

We used apatite (U-Th)/He (AHe) and apatite fission-track (AFT) ages, determined for plutons throughout the Klamath Mountain province, to place constraints on the timing, duration, and amount of exhumation in the central Klamath Mountain province. We have included samples from the footwall and hanging wall of the La Grange fault, from plutons northwest of the inferred fault extent, and from a conglomerate deposited synchronously with faulting. Our samples (Table 1) extend over a wider area and range of structural settings than those in the geographically focused study of Batt et al. (2010b), and they allow us to better constrain the extent and timing of the La Grange fault extension (Fig. 3; Tables 1, 2, and 3).

Thermochronometry Results

AFT and AHe ages were determined for a suite of samples from within the Klamath Mountain province, including samples for the hanging wall and footwall of the La Grange fault and exposed plutons outside the fault extent (Table 1). Analytical procedures for apatite fission-track analysis and AHe dating are described in the Appendix.

AFT ages vary systematically with geographic and structural position. AFT age and

TABLE 1. SAMPLE NAMES AND LOCATIONS

Pluton	Sample code	Latitude (°N)	Longitude (°W)
Craggy Peak	CP-02	41.2485	122.8167
	CP-03	41.2597	122.8135
	CP-05	41.2717	122.7944
Sugar Pine	SP-01	41.1071	122.8013
	SP-05	41.0586	122.7518
	SP-06	41.0319	122.7572
Granite Peak	GP-01	40.8566	122.8844
	GP-02	40.8954	122.8546
Russian Peak	RP-01	41.4324	122.9347
	RP-02	41.4290	122.9647
	RP-04	41.2753	122.9181
Caribou Mountain	CM-03	41.0486	122.9568
Canyon Creek	CC-01	40.9331	123.0216
	CC-02	40.9298	123.0208
	CC-03	40.9131	123.0226
Monument Peak	MP-01	40.8300	122.9800
Wooley Creek	WC-01	41.4160	123.3986
	WC-05	41.6586	123.3164
Slinkard	SL-02	41.8153	123.1549
Shasta Bally	SB-01	40.6653	122.7883
	SB-03	40.6577	122.7673
Mule Mountain	MM-01	40.6000	122.5350
Weaverville Formation (pluton-derived clast)	WV-02a	–	–

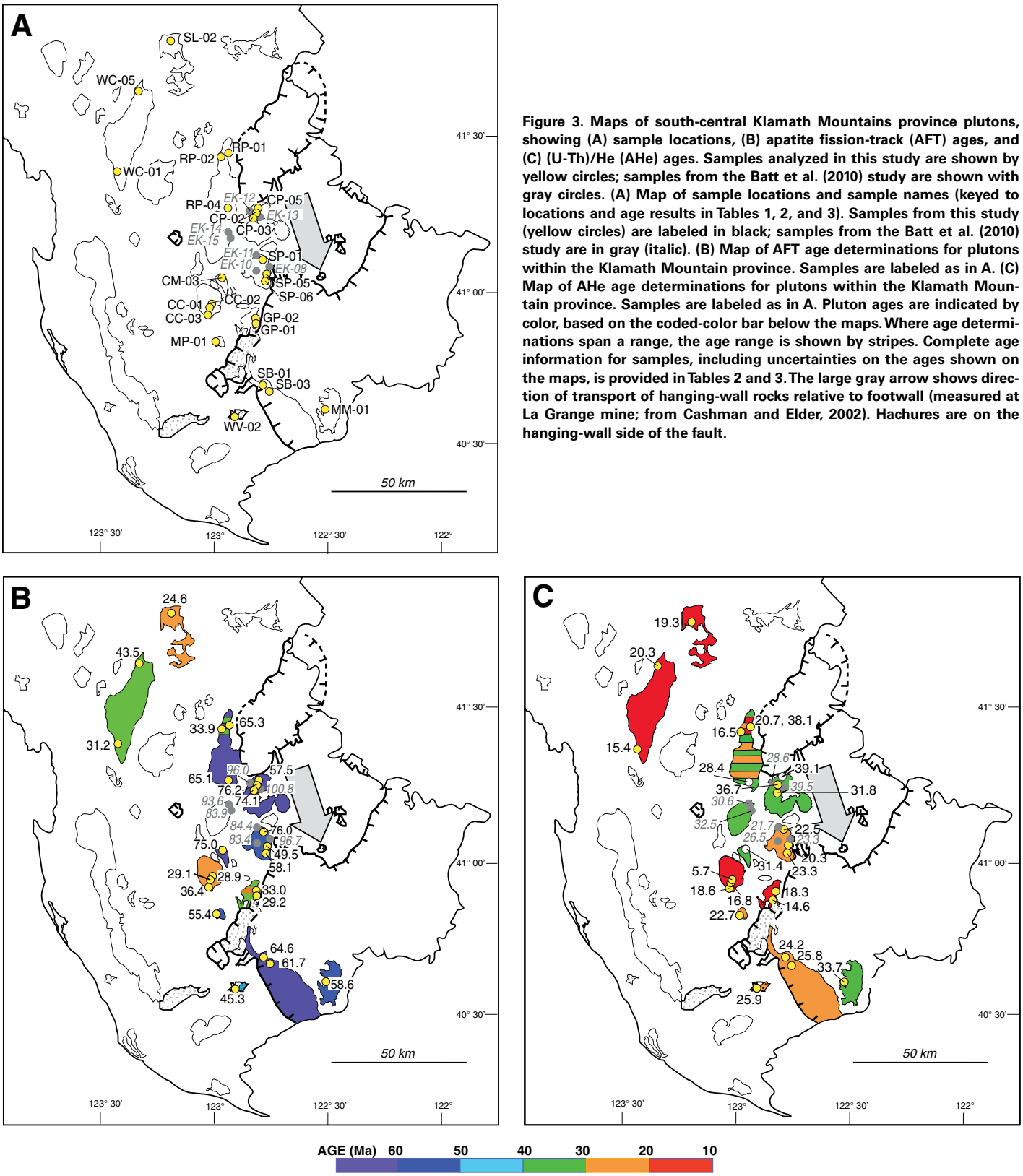

Figure 3. Maps of south-central Klamath Mountains province plutons, showing (A) sample locations, (B) apatite fission-track (AFT) ages, and (C) (U-Th)/He (AHe) ages. Samples analyzed in this study are shown by yellow circles; samples from the Batt et al. (2010) study are shown with gray circles. (A) Map of sample locations and sample names (keyed to locations and age results in Tables 1, 2, and 3). Samples from this study (yellow circles) are labeled in black; samples from the Batt et al. (2010) study are in gray (italic). (B) Map of AFT age determinations for plutons within the Klamath Mountain province. Samples are labeled as in A. (C) Map of AHe age determinations for plutons within the Klamath Mountain province. Samples are labeled as in A. Pluton ages are indicated by color, based on the coded-color bar below the maps. Where age determinations span a range, the age range is shown by stripes. Complete age information for samples, including uncertainties on the ages shown on the maps, is provided in Tables 2 and 3. The large gray arrow shows direction of transport of hanging-wall rocks relative to footwall (measured at La Grange mine; from Cashman and Elder, 2002). Hachures are on the hanging-wall side of the fault.

TABLE 2. APATITE FISSION-TRACK DATA

Sample field number	Number of crystals	Spontaneous		Induced		$P(\chi^2)$ %	ρ_d	N_d	Age (Ma ± 1σ)	Mean track length (μm ± 1σ)	Standard deviation (μm)	Number of lengths
		ρ_s	N_s	ρ_i	N_i							
Samples west of La Grange fault												
WC-01	20	0.252	75	1.866	556	100	1.329	3153	31.2 ± 3.9	14.02 ± 0.18	0.86	23
WC-05	20	2.532	776	14.263	4372	15.0	1.411	3348	43.5 ± 2.0	13.02 ± 0.12	1.20	101
SL-02	20	0.768	207	7.762	2092	98.7	1.428	3387	24.6 ± 1.9	14.18 ± 0.23	1.40	38
La Grange fault footwall												
RP-01	20	0.352	117	1.213	403	100	1.296	3074	65.3 ± 7.0	13.28 ± 0.19	1.41	55
RP-02	20	0.304	51	1.863	313	100	1.197	2840	33.9 ± 5.2	14.03 ± 0.33	1.19	13
RP-04	20	0.564	212	1.786	671	100	1.122	2663	61.5 ± 5.1	13.17 ± 0.22	1.75	64
CP-02	20	0.380	196	1.093	563	99.6	1.263	2996	76.2 ± 6.6	13.50 ± 0.22	1.43	41
CP-03	20	0.540	229	1.657	703	100	1.312	3113	74.1 ± 5.9	13.46 ± 0.20	1.47	55
CP-05	20	0.655	164	2.335	585	83.6	1.181	2801	57.5 ± 5.3	13.25 ± 0.22	1.44	44
CM-03	20	1.097	714	3.536	2302	28.2	1.395	3309	75.0 ± 3.7	13.16 ± 0.17	1.42	66
CC01	20	0.226	142	2.238	654	99.9	1.246	2957	21.9 ± 2.9	12.60 ± 2.07	3.58	3
CC-02	20	0.270	151	2.341	1311	99.9	1.444	3426	28.9 ± 2.6	13.86 ± 0.21	1.48	51
CC-03	20	0.270	110	1.436	586	99.5	1.114	2643	36.4 ± 3.9	13.92 ± 0.22	1.65	56
MP-01	20	0.132	94	0.507	362	100	1.239	2916	55.4 ± 6.6	12.91 ± 0.85	2.82	11
SP-01	20	1.282	607	3.360	1591	92.4	1.149	2726	76.0 ± 4.1	13.99 ± 0.16	1.28	62
SP-05	20	0.431	137	1.862	592	99.9	1.230	2918	49.5 ± 4.8	13.56 ± 0.19	1.51	65
SP-06	20	1.734	423	6.187	1509	96.9	1.193	2831	58.1 ± 3.5	13.08 ± 0.25	1.84	54
GP-01	20	0.465	142	3.227	986	96.2	1.164	2762	29.2 ± 2.7	13.86 ± 0.13	1.08	65
GP-02	20	0.377	74	2.540	499	97.0	1.279	3035	33.0 ± 4.2	14.72 ± 0.24	1.20	26
La Grange fault hanging wall												
SB-01	20	0.767	233	2.404	730	99.9	1.167	2768	64.6 ± 5.1	12.79 ± 0.22	1.77	67
SB-03	20	0.620	365	2.347	1381	90.0	1.345	3192	61.7 ± 3.9	13.19 ± 0.28	2.20	64
MM-01	20	0.534	268	1.833	920	73.7	1.158	2747	58.6 ± 4.3	14.85 ± 0.35	1.43	17
WV-02a	20	1.070	340	4.979	1583	96.4	1.214	2879	45.3 ± 2.9	12.89 ± 0.18	1.78	100
8122-3*	20	0.186	177	1.352	1287	99.7	1.256	2979	30.1 ± 2.5			

Note: ρ_s (ρ_i)—spontaneous (induced) track densities (×10^6 tracks/cm^2); N_s (N_i)—number of counted spontaneous (induced) tracks; ρ_d—dosimeter track density (×10^5 tracks/cm^2); N_d—number of tracks counted on dosimeter; $P(\chi^2)$—probability obtaining Chi-square value (χ^2) for *n* degree of freedom (where *n* = No. of crystals – 1; Galbraith, 1981). All analyses are by the external detector method. Apatite ages were calculated using dosimeter glass CN5 and zeta-612 = 348.8 ± 5.5 (±1σ) by Ganqing Xu. Central AFT ages and related uncertainties are calculated after Galbraith and Green (1990).

*Durango Apatite age = 31.4 ± 0.5 Ma.

length data were acquired for 23 samples from 11 plutons and from one clast collected from Weaverville Formation conglomerate (Table 2; Fig. 3B). The three samples northwest of the La Grange fault have relatively young AFT ages, ranging from ca. 45 to 25 Ma (Table 2; Fig. 3B). Samples from the La Grange fault hanging wall have AFT ages in the range ca. 65–59 Ma, while those from the footwall show a significant range from ca. 76 to 22 Ma (Table 2). The AFT age of the diorite clast from the Weaverville Formation in the Reading Creek graben is ca. 26 Ma.

AFT ages record moderate to rapid cooling. The track length distributions are uniformly unimodal, with mean track lengths in the range of 12.7–14.9 μm, irrespective of structural position of the host plutons. This indicates that most of the fission-track ages record moderate to rapid regional cooling of the sample host rocks into and through the AFT partial annealing zone during the Late Cretaceous and Paleogene. The younger AFT ages (Eocene and younger) probably reflect cooling through the partial annealing zone during and soon after detachment faulting. Our fission-track ages are in general agreement (Cretaceous–Paleocene) with those reported in Batt et al. (2010b), although where the same plutons (Russian Peak, Craggy Peak) were sampled in both studies, albeit not the same locations, our ages are consistently younger (Fig. 3B).

AHe ages vary systematically with geographic and structural position. Reproducibility of replicates in the majority of samples is excellent, with most overlap within 1σ level of uncertainty. We determined AHe ages for 110 single apatite crystals from 23 samples representing 11 plutons and one clast collected from Weaverville Formation conglomerate in Reading Creek graben (Table 3; Fig. 3C). Only one sample (RP-01, Russian Peak pluton) yielded two groups of AHe ages that do not overlap. Single-grain AHe ages range from 2.6 ± 0.2 Ma to 44.3 ± 2.7 Ma, and all overlap or are younger than the corresponding AFT ages, in agreement with the closure temperature concept (Dodson, 1973). Our results for plutons (Russian Peak, Craggy Peak) also sampled in Batt et al. (2010b) are statistically indistinguishable from results in that study (Fig. 3C).

AHe ages vary systematically within the footwall of the La Grange fault, as observed by Batt et al. (2010b), and they also record distinct contrasts between the footwall and hanging wall, and between both fault blocks and rocks northwest of the fault. Plutons in the footwall show a southward progression of successively younger ages and span a wide range, including both older and younger AHe ages than hanging-wall samples (Figs. 3C and 4). AHe ages from hanging-wall samples (Shasta Bally and Mule Mountains plutons) range from ca. 34 to ca. 24 Ma, and the clast from conglomerate preserved in the Reading Creek graben has a comparable AHe age of ca. 26 Ma (Table 3; Fig. 3C). AHe ages from the "Trinity arch" central region of the La Grange fault footwall range from older than those in the hanging wall for the most northern pluton (Craggy Peak, ca. 40–32 Ma) to overlapping those of hanging-wall rocks (Deadman Peak and Caribou Mountain plutons, ca. 33–30 Ma; Sugar

Pine pluton, 27–20 Ma). The youngest AHe ages, ca. 15–6 Ma, are found in the Granite Peak and Canyon Creek plutons in the southernmost part of the footwall and close to the outcrop trace of the fault. AHe ages for samples in the northwesternmost part of the study area are comparable to those of the youngest rocks in the study region; the Wooley Creek–Slinkard intrusive complex has AHe ages of ca. 20–15 Ma.

These new thermochronology data record two tectonically distinct periods of exhumation—a Late Cretaceous–Paleocene interval of regional (erosional?) cooling and exhumation seen in the AFT ages both within and external to the geographic extent of the La Grange fault, and a middle Tertiary (Oligocene–Miocene), systematically spatially varying period of rapid cooling of the La Grange fault footwall, seen primarily in the AHe ages. This latter event reflects a southward-migrating locus of rapid cooling/exhumation in middle Tertiary time (Figs. 4 and 5); this event is interpreted as the signature of detachment faulting on the La Grange fault (Batt et al., 2010b; this study). New data and thermal modeling based on the new age data are consistent with the following sequence of events (Figs. 4 and 5): initiation of exhumation ca. 45 Ma, progressing southward across Russian Peak pluton and Craggy Peak pluton until ca. 35 Ma, and continuing past Caribou Mountain pluton ca. 35–30 Ma, the Sugar Pine pluton ca. 23–21 Ma, and the Granite Peak pluton ca. 19–16 Ma (Piotraschke, 2012, p. 33). The zone of southward-progressing exhumation is bordered by regions with relatively uniform late Oligocene to early Miocene (20–30 Ma) AHe ages independent of north-south position (Figs. 3C, 4, and 5). We infer that the pattern of this middle Tertiary event reflects two distinct processes of exhumation: migrating localized fault exhumation of the footwall of the La Grange detachment fault, and continued regional surface erosion both east and west of the LaGrange fault extent.

Kinematics of Fault Exhumation

The conditions and duration of faulting on the La Grange fault differ from those of other detachment faults. Thermochronologic data from the La Grange fault footwall combined with microstructural observations from fault rocks at the LaGrange mine imply that faulting occurred entirely at shallow (brittle deformation) depths (Cashman and Cashman, 2006), persisted for ~30 m.y., and occurred at a relatively slow slip rate (average ~2 mm/yr). This average slip rate is unusually low, and the duration of faulting (~30 m.y.) is remarkably long compared to values reported for other detachment faults. For comparison, an average slip rate of 6–8 km/m.y.

TABLE 3. APATITE (U-Th)/He RESULTS

Sample code		Th (ng)	± (%)	U (ng)	± (%)	He (ncc)	± (%)	TAU (%)	Th/U	Uncorr. age (Ma)	±1σ (Ma)	F_t	Corr. age (Ma)	±1σ (Ma)
SAMPLES WEST OF LA GRANGE FAULT														
Wooley Creek														
WC-01	a	0.038	3.9	0.022	4.2	0.036	3.5	4.8	1.68	9.4	0.4	0.60	15.7	1.1
	b	0.025	4.0	0.018	4.5	0.026	1.5	3.8	1.40	8.9	0.3	0.53	16.9	1.8
	c	0.025	4.0	0.012	4.8	0.017	0.6	3.6	2.05	7.9	0.3	0.58	13.6	1.4
	d	0.025	3.9	0.017	4.3	0.024	0.8	3.5	1.47	8.9	0.3	0.56	15.8	1.7
	e	0.037	3.9	0.025	4.5	0.039	0.6	3.5	1.48	9.5	0.3	0.62	15.3	0.9
										Central age ± st. dev. (both in Ma):			15.4 ±	1.2
WC-05	a	0.163	3.8	0.150	4.2	0.231	0.5	3.5	1.08	10.1	0.3	0.53	19.1	2.0
	b	0.268	3.8	0.249	4.3	0.467	0.5	3.6	1.07	12.3	0.4	0.64	19.1	1.2
	c	0.393	3.8	0.448	4.1	0.983	0.5	3.5	0.87	14.9	0.5	0.68	21.9	1.3
	d	0.214	3.8	0.322	4.8	0.568	0.6	4.2	0.66	12.5	0.5	0.63	20.0	1.3
	e	0.197	3.8	0.304	4.4	0.457	0.6	3.9	0.64	10.7	0.4	0.58	18.5	2.0
	f	0.204	3.8	0.317	5.6	0.633	0.5	4.9	0.64	14.2	0.7	0.66	21.5	1.5
										Central age ± st. dev. (both in Ma):			20.3 ±	1.4
Slinkard														
SL-02	a	0.018	4.1	0.038	4.3	0.043	0.5	3.9	0.48	8.5	0.3	0.51	16.7	1.8
	b	0.042	3.9	0.076	4.3	0.133	0.5	3.8	0.55	12.8	0.5	0.61	20.9	1.3
	c	0.012	4.2	0.075	4.1	0.093	0.5	4.0	0.16	9.8	0.4	0.54	18.3	2.0
	d	0.056	3.8	0.102	4.2	0.180	0.5	3.8	0.54	12.8	0.5	0.63	20.4	1.3
	e	0.059	3.8	0.117	4.2	0.186	0.5	3.8	0.50	11.7	0.4	0.65	18.0	1.1
	f	0.047	3.9	0.069	4.9	0.113	0.6	4.3	0.68	11.6	0.5	0.59	19.6	2.1
										Central age ± st. dev. (both in Ma):			19.3 ±	1.6
LA GRANGE FAULT FOOTWALL														
Russian Peak														
RP-01	*a*	*0.021*	*3.7*	*0.016*	*4.0*	*0.055*	*1.2*	*3.4*	*1.29*	*21.9*	*0.8*	*0.60*	*36.6*	*2.2*
	b	*0.039*	*3.7*	*0.025*	*4.0*	*0.095*	*1.2*	*3.3*	*1.52*	*22.4*	*0.7*	*0.56*	*39.8*	*2.4*
	c	0.040	3.7	0.015	4.0	0.035	1.2	3.1	2.69	11.9	0.4	0.55	21.7	1.3
	d	0.033	3.7	0.010	4.0	0.029	1.3	3.1	3.23	13.1	0.4	0.66	19.9	1.2
										Central age ± st. dev. (both in Ma):			20.7 ±	1.3
										Central age ± st. dev. (both in Ma):			38.1 ±	2.3
RP-02	a	0.041	3.6	0.081	3.9	0.106	1.3	3.8	0.51	9.6	0.4	0.66	14.6	0.9
	b	0.005	5.5	0.014	4.1	0.015	1.6	4.1	0.34	7.8	0.3	0.50	15.7	1.0
	c	*0.008*	*4.9*	*0.006*	*4.4*	*0.011*	*1.3*	*3.7*	*1.38*	*12.2*	*0.5*	*0.52*	*23.4*	*3.6*
	d	0.022	4.0	0.005	4.5	0.013	0.9	3.1	4.17	9.9	0.3	0.56	17.8	2.7
										Central age ± st. dev. (both in Ma):			16.5 ±	3.9
RP-04	a	0.069	3.8	0.047	4.0	0.114	0.7	3.2	1.44	14.8	0.5	0.58	25.7	1.5
	b	0.040	3.9	0.023	4.0	0.073	0.9	3.2	1.70	18.3	0.6	0.65	28.1	1.7
	c	0.046	3.8	0.038	4.1	0.111	0.7	3.3	1.20	18.4	0.6	0.68	27.2	1.6
	d	0.051	3.9	0.032	4.1	0.112	0.5	3.2	1.59	21.1	0.7	0.64	33.1	2.0
										Central age st. dev. (both in Ma):			28.4 ±	3.2
Craggy Peak														
CP-02	a	0.026	3.7	0.019	4.0	0.071	1.5	3.5	1.33	23.0	0.8	0.65	35.6	2.2
	b	0.031	3.7	0.024	3.9	0.085	1.4	3.4	1.32	22.4	0.8	0.64	34.8	2.1
	c	0.026	3.7	0.015	3.9	0.068	1.5	3.3	1.69	25.8	0.9	0.66	39.2	2.4
	d	0.073	3.6	0.067	3.9	0.341	1.3	3.5	1.08	33.3	1.1	0.76	43.6	2.7
	e	0.030	3.7	0.025	4.4	0.079	1.6	3.8	1.19	20.5	0.8	0.65	31.4	2.0
										Central age ± st. dev. (both in Ma):			36.7 ±	4.7
CP-03	a	0.033	3.7	0.025	4.1	0.075	1.6	3.6	1.32	18.8	0.7	0.62	30.5	1.9
	b	*0.036*	*3.7*	*0.020*	*3.9*	*0.116*	*1.5*	*3.3*	*1.81*	*33.8*	*1.1*	*0.76*	*44.3*	*2.7*
	c	0.075	3.6	0.044	3.9	0.187	1.4	3.3	1.69	24.8	0.8	0.77	32.3	1.9
	d	0.033	3.7	0.025	4.0	0.079	1.6	3.5	1.31	19.7	0.7	0.64	30.6	1.9
	e	0.041	3.7	0.032	4.0	0.127	1.5	3.5	1.29	25.3	0.9	0.75	33.8	2.1
										Central age ± st. dev. (both in Ma):			31.8 ±	1.6
CP-05	a	0.043	3.6	0.025	3.9	0.113	1.6	3.4	1.76	26.6	0.9	0.68	39.1	2.4
	b	0.042	3.7	0.024	3.9	0.110	1.7	3.4	1.69	26.4	0.9	0.66	40.3	2.4
	c	0.087	3.6	0.048	3.9	0.249	1.6	3.4	1.79	29.7	1.0	0.76	39.0	2.4
	d	0.063	3.6	0.030	4.0	0.153	1.6	3.4	2.07	27.7	0.9	0.73	38.0	2.3
	e	0.058	3.8	0.029	4.0	0.139	1.6	3.4	2.02	26.9	0.9	0.69	39.0	2.4
										Central age ± st. dev. (both in Ma):			39.1 ±	0.8
Caribou Mountain														
CM-03	a	0.011	4.4	0.014	4.2	0.050	1.1	3.8	0.74	24.2	0.9	0.71	34.1	2.1
	b	0.016	4.1	0.031	4.1	0.081	0.5	3.7	0.52	19.1	0.7	0.60	31.9	2.0
	c	0.013	4.2	0.014	4.0	0.037	0.6	3.4	0.92	18.2	0.6	0.60	30.5	1.9
	d	0.013	4.1	0.017	4.1	0.043	0.6	3.6	0.76	18.0	0.6	0.62	29.2	1.8
										Central age ± st. dev. (both in Ma):			31.4 ±	2.1
Canyon Creek														
CC-01	a	0.042	3.7	0.053	3.9	0.039	1.3	3.6	0.79	5.0	0.2	0.68	7.4	0.5
	b	0.048	3.6	0.039	4.0	0.033	1.3	3.5	1.21	5.4	0.2	0.68	7.8	0.5
	c	0.080	3.6	0.063	3.9	0.019	1.6	3.5	1.27	1.9	0.1	0.75	2.6	0.2
	d	0.026	3.7	0.026	4.0	0.016	1.3	3.6	1.01	4.1	0.1	0.62	6.5	0.4
	e	0.036	3.7	0.032	4.0	0.014	1.4	3.5	1.14	2.8	0.1	0.65	4.2	0.3
	f	0.013	5.2	0.013	5.3	0.003	1.2	4.5	1.01	1.3	0.1	0.51	2.6	0.3
	g	0.014	4.0	0.009	4.2	0.006	1.1	3.4	1.62	4.1	0.1	0.53	7.8	0.8
	h	0.038	4.1	0.031	5.0	0.026	1.0	4.1	1.21	5.4	0.2	0.65	8.3	0.5
	i	0.051	3.9	0.037	4.4	0.036	0.5	3.5	1.37	6.1	0.2	0.70	8.7	0.5
										Central age ± st. dev. (both in Ma):			5.7 ±	2.4

(*continued*)

TABLE 3. APATITE (U-Th)/He RESULTS (*continued*)

Sample code		Th (ng)	± (%)	U (ng)	± (%)	He (ncc)	± (%)	TAU (%)	Th/U	Uncorr. age (Ma)	±1σ (Ma)	F_t	Corr. age (Ma)		±1σ (Ma)
Canyon Creek (*continued*)															
CC-02	a	0.041	4.0	0.024	4.4	0.042	0.6	3.4	1.71	10.4	0.3	0.56	18.6		2.0
	b	0.033	3.9	0.020	4.7	0.034	0.6	3.6	1.58	9.8	0.4	0.60	16.3		1.0
									Central age ± st. dev. (both in Ma):				16.8	±	1.6
CC-03	a	0.017	4.0	0.007	4.2	0.016	2.1	3.7	2.26	11.8	0.4	0.61	19.2		1.2
	b	0.056	3.9	0.029	4.0	0.059	0.6	3.1	1.92	11.5	0.4	0.67	17.2		1.0
	c	0.042	3.9	0.023	4.1	0.051	0.5	3.1	1.83	13.0	0.4	0.66	19.6		1.2
	d	0.031	3.9	0.020	4.0	0.040	0.5	3.2	1.55	11.9	0.4	0.64	18.6		1.1
	e	0.025	4.0	0.017	4.1	0.032	0.6	3.2	1.47	11.4	0.4	0.60	18.9		1.1
									Central age ± st. dev. (both in Ma):				18.6	±	0.9
Monument Peak															
MP-01	a	0.010	4.6	0.006	4.2	0.013	1.3	3.5	1.70	14.0	0.5	0.62	22.5		1.4
	b	0.013	4.1	0.007	4.0	0.019	1.7	3.5	1.79	14.8	0.5	0.62	23.8		1.5
	c	*0.025*	*3.9*	*0.017*	*4.1*	*0.020*	*1.6*	*3.6*	*1.45*	*7.1*	*0.3*	*0.69*	*10.4*		*0.6*
	d	0.014	4.1	0.012	4.1	0.026	1.5	3.6	1.15	14.4	0.5	0.63	22.7		1.4
	e	0.006	4.6	0.004	4.1	0.008	4.3	5.4	1.68	12.6	0.7	0.58	21.7		1.6
									Central age ± st. dev. (both in Ma):				22.7	±	0.9
Sugar Pine															
SP-01	a	0.036	3.9	0.013	4.2	0.032	1.5	3.3	2.76	12.4	0.4	0.58	21.1		1.3
	b	0.028	3.9	0.014	4.1	0.032	2.0	3.7	2.00	12.9	0.5	0.61	21.4		1.3
	c	0.079	3.8	0.038	4.0	0.100	0.9	3.1	2.05	14.4	0.4	0.59	24.3		1.4
	d	0.107	3.8	0.057	4.0	0.150	0.8	3.1	1.86	14.9	0.5	0.65	23.0		1.4
									Central age ± st. dev. (both in Ma):				22.5	±	1.5
SP-05	a	0.051	3.7	0.020	4.0	0.049	1.4	3.2	2.54	12.5	0.4	0.58	21.7		1.3
	b	0.036	3.7	0.013	4.6	0.030	1.5	3.4	2.80	11.4	0.4	0.63	18.0		1.1
	c	0.051	3.6	0.019	3.9	0.048	1.4	3.1	2.72	13.0	0.4	0.63	20.7		1.2
	d	0.071	3.6	0.027	4.0	0.074	1.3	3.1	2.65	14.0	0.4	0.67	20.9		1.2
									Central age ± st. dev. (both in Ma):				20.3	±	1.6
SP-06	a	0.246	3.8	0.152	4.1	0.400	0.5	3.2	1.60	15.6	0.5	0.66	23.7		1.4
	b	0.162	3.8	0.111	4.1	0.313	0.5	3.2	1.46	17.2	0.6	0.73	23.5		1.4
	c	0.250	3.8	0.156	4.1	0.414	0.5	3.2	1.59	15.8	0.5	0.66	24.1		1.4
	d	0.157	3.8	0.101	4.0	0.225	0.5	3.1	1.54	13.4	0.4	0.62	21.7		1.3
	e	0.170	3.8	0.115	4.1	0.260	0.5	3.3	1.47	13.8	0.4	0.59	23.4		1.4
									Central age ± st. dev. (both in Ma):				23.3	±	0.9
Granite Peak															
GP-01	a	0.093	5.3	0.128	5.4	0.201	1.7	5.0	0.72	11.0	0.5	0.69	16.0		1.1
	b	0.059	3.6	0.080	3.9	0.119	1.6	3.8	0.73	10.4	0.4	0.70	14.8		0.9
	c	0.066	3.6	0.085	3.9	0.116	1.7	3.8	0.77	9.5	0.4	0.72	13.2		0.8
	d	0.017	3.7	0.049	4.0	0.062	1.7	4.1	0.35	9.6	0.4	0.68	14.0		0.9
	e	0.080	3.6	0.099	4.0	0.135	1.7	3.8	0.81	9.4	0.4	0.62	15.3		1.0
									Central age ± st. dev. (both in Ma):				14.6	±	1.1
GP-02	a	0.060	3.6	0.038	4.0	0.084	1.2	3.3	1.56	13.3	0.4	0.69	19.3		1.2
	b	0.043	3.7	0.026	4.0	0.040	1.2	3.3	1.63	9.2	0.3	0.58	15.8		0.9
	c	0.019	3.7	0.011	4.0	0.018	1.3	3.3	1.74	9.6	0.3	0.59	16.4		1.0
	d	0.032	3.7	0.017	4.0	0.035	1.3	3.2	1.89	12.1	0.4	0.55	21.8		1.3
	e	*0.018*	*3.7*	*0.019*	*4.1*	*0.057*	*1.2*	*3.7*	*0.93*	*19.9*	*0.7*	*0.61*	*32.8*		*2.0*
	f	0.038	3.9	0.019	4.3	0.035	0.5	3.2	1.96	10.1	0.3	0.53	19.2		2.0
									Central age ± st. dev. (both in Ma):				18.3	±	2.4
LA GRANGE FAULT HANGING WALL															
Shasta Bally															
SB-01	a	0.037	4.1	0.016	4.6	0.036	0.5	3.4	2.32	11.9	0.4	0.49	24.5		2.6
	b	0.056	3.8	0.026	4.7	0.075	0.5	3.4	2.14	15.7	0.5	0.59	26.6		2.8
	c	0.064	3.9	0.031	4.7	0.071	0.5	3.4	2.07	12.7	0.4	0.56	22.6		2.4
	d	0.060	3.8	0.033	4.2	0.090	0.5	3.2	1.83	15.8	0.5	0.61	25.7		1.5
	e	0.118	3.8	0.057	4.4	0.154	0.5	3.2	2.04	14.9	0.5	0.66	22.4		1.3
									Central age ± st. dev. (both in Ma):				24.2	±	1.9
SB-03	a	0.059	3.9	0.030	4.6	0.091	1.4	3.6	1.96	17.1	0.6	0.64	26.9		1.7
	b	0.051	3.9	0.028	4.7	0.073	0.6	3.5	1.82	15.0	0.5	0.58	25.8		2.7
	c	0.067	3.8	0.033	4.4	0.092	0.5	3.3	2.00	15.3	0.5	0.59	25.8		2.7
	d	0.043	3.9	0.022	4.2	0.058	0.5	3.2	1.91	14.6	0.5	0.59	24.7		2.6
									Central age ± st. dev. (both in Ma):				25.8	±	0.9
Mule Mountain															
MM-01	a	0.037	3.9	0.016	4.3	0.065	0.9	3.2	2.28	21.5	0.7	0.64	33.7		2.0
Weaverville Formation															
WV-02a	a	0.042	3.7	0.075	3.9	0.201	1.7	3.9	0.56	19.5	0.8	0.67	29.2		1.8
	b	*0.027*	*3.7*	*0.066*	*3.9*	*0.083*	*1.6*	*4.0*	*0.41*	*9.4*	*0.4*	*0.57*	*16.5*		*1.1*
	c	0.029	3.7	0.041	4.0	0.098	1.7	3.9	0.71	16.9	0.7	0.61	27.8		1.8
	d	0.018	4.1	0.011	4.0	0.028	1.3	3.4	1.70	15.1	0.5	0.65	23.3		1.4
	e	0.056	3.6	0.076	4.0	0.170	1.4	3.7	0.73	15.7	0.6	0.66	23.8		1.5
									Central age ± st. dev. (both in Ma):				25.9	±	2.9

Note: Th—^{232}Th; U—^{238}U; He—^{4}He at standard temperature and pressure; TAU—total analytical uncertainty; Uncorr. age—uncorrected He age; F_t—alpha recoil correction factor after Farley et al. (1996); Cor. age—corrected He age. Ages in *italics* are outliers and were omitted from calculation of central age.

for ~8 m.y. is reported for the Naxos-Paros extensional fault system in Greece (Brichau et al. 2006), and slip rates accelerating from ~1.6 km/m.y. to ~6 km/m.y. over a span of ~20 m.y. are calculated for the southern California Chemehuevi detachment (Carter at al., 2006).

The fault surface exposed at the La Grange mine is significantly steeper than its dip over most of its regional extent. The exposed surface of the fault at the LaGrange mine dips southward at ~20°, but our thermochronologic data require that over the entire extent of the fault, its average dip must be significantly shallower (5° or less), and the upper-plate thickness must be less than ~6–8 km. This interpretation of fault geometry is consistent with the presence of highly comminuted brittle fault rocks (foliated ultracataclasite) on the fault surface and with the occurrence of calcite and (rare) calcite-heulandite veins crosscutting foliation in the ultracataclasite (Cashman and Cashman, 2006). The presence of heulandite shows that veins formed at pressure-temperature conditions no higher than 200–400 MPa and 240 ± 40 °C (Frey et al., 1991), correlating to a maximum depth of 7 km. Small clusters of prismatic heulandite crystals radiating inward from vein walls appear to have grown in the absence of neighbors, suggesting that crystallization occurred in the shallower part of the heulandite stability range (Cashman and Cashman, 2006).

In summary, the thermal-tectonic history for the Klamath Mountain province is:

(1) Based on AFT results, currently exposed plutons in the southeastern Klamath Mountain province were exhumed from initial emplacement depths to moderately shallow levels in the crust (<~120 °C; <~6–8 km depth) during Late Cretaceous–Paleocene time.

(2) In contrast, AFT data from plutons in the central Klamath Mountain province (Wooley Creek–Slinkard complex) indicate they underwent exhumation and cooling to below ~120 °C in Oligocene time. This difference may reflect either a greater emplacement depth or slower exhumation for these plutons.

(3) Based on AHe results, there was a southward-migrating locus of rapid cooling/exhumation in the La Grange fault footwall that moved ~60 km between 45 and 15 Ma, recording an average fault slip rate of ~2 km/m.y. over ~30 m.y.

(4) Although some post–La Grange fault erosion has occurred (as no fault rocks are observed in the exhumed footwall except in the vicinity of the La Grange mine), displacement in response to slip on the La Grange fault was responsible for a substantial amount, and perhaps the majority, of exhumation within the Trinity arch region of the Klamath Mountain province.

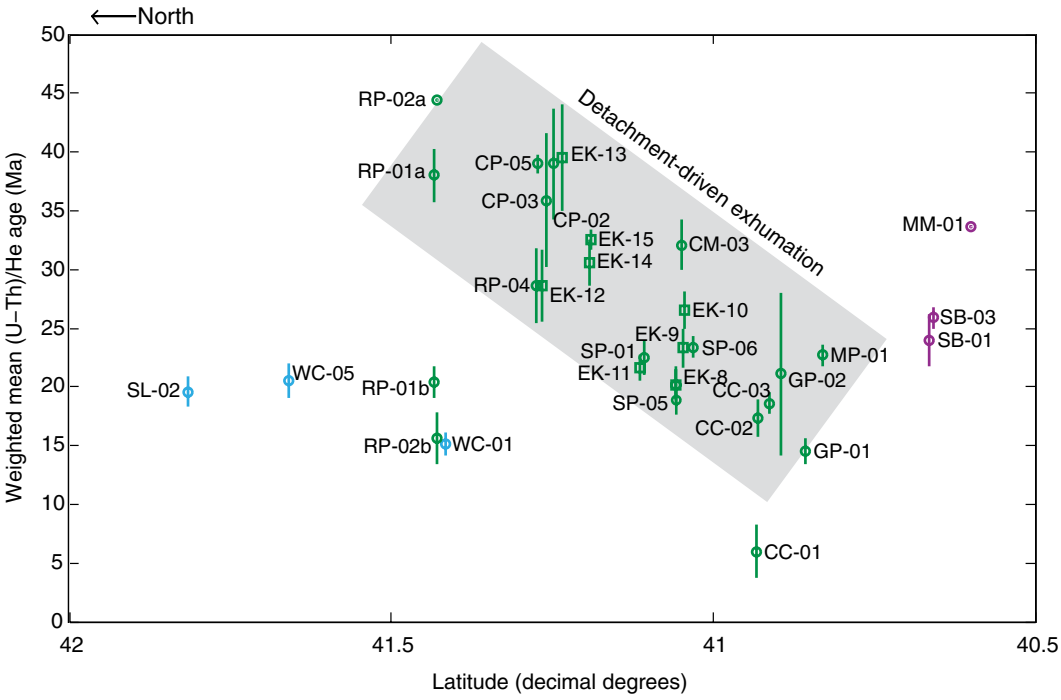

Figure 4. Plot of AHe ages relative to latitude. Color indicates setting of sample: blue—outside of region of La Grange fault; green—La Grange fault footwall; purple—La Grange fault hanging wall. Circle—data from this study, square—data from Batt et al. (2010b). Gray box outlines north-to-south pattern of ages exposed by the detachment faulting.

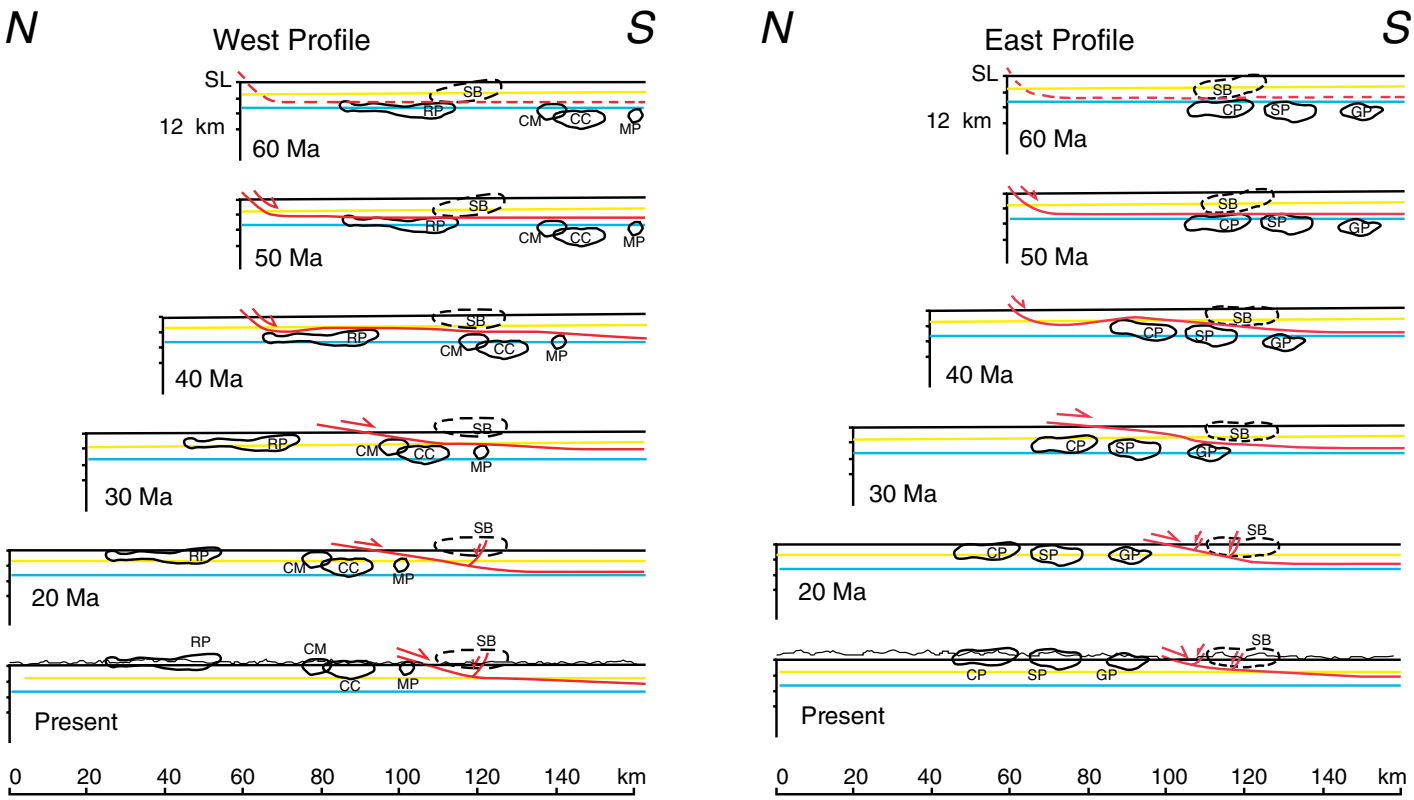

Figure 5. Schematic illustration of La Grange detachment faulting over time. Two north-south–trending cross sections are shown: west profile: starting at Russian Peak pluton (longitude ~123°W), and east profile: starting at Craggy Peak pluton (longitude ~122°45′W). Plutons shown are Canyon Creek (CC), Caribou Mountain (CM), Craggy Peak (CP), Granite Peak (GP), Monument Peak (MP), Shasta Bally (SB), Sugar Pine (SP), and Russian Peak (RP). Dashed outline of Shasta Bally batholith indicates approximate extent of the batholith, projected westward onto the line of section. Timing of exhumation shown is guided by approximate apatite fission-track (~6.5 km, blue line) and (U-Th)/He (~3 km, yellow line) closure or annealing depths and ages for individual plutons. No vertical exaggeration. Topography shown is schematic.

Link to Western North America Tectonics

Implications for Neogene Deformation in the Klamath Mountains Province

Thermochronology results presented here place new limits on two prior interpretations of Neogene tectonics of the Klamath Mountain province: the Condrey Mountain dome (Mortimer and Coleman, 1985) and the tilted Klamath peneplain (Diller, 1902; Aalto, 2006).

Mortimer and Coleman (1985) proposed that Neogene domal uplift centered on Condrey Mountain had occurred in the northeastern Klamath Mountain province, based largely on a subannular outcrop pattern of stacked, subhorizontal bedrock units, southwestward tilting of the Wooley Creek–Slinkard plutonic system southwest of Condrey Mountain, and tilted Cretaceous to Miocene strata on the east and west margins of the Klamath Mountain province at the latitude of Condrey Mountain. Further studies substantiated this structural interpretation (e.g., Barnes et al., 1986) and presented evidence for 6 km of differential uplift of the Condrey Mountain dome (Jachens et al., 1986) but did not further address the timing or mechanism of doming. AFT ages for the Slinkard–Wooley Creek plutonic system show that the bulk of rock uplift occurred before mid-Miocene time and demonstrate that the ~6 km of structural relief on the Condrey Mountain dome reported by Jachens et al. (1986) cannot all be of Neogene age. The Slinkard pluton (closest to the center of the Condrey Mountain dome) was uplifted from its Late Jurassic emplacement depth of >30 km (Barnes et al., 1986) to ~7 km depth by the late Oligocene (AFT age 24.6 ± 1.9) and to within 3 km of the surface by the early Miocene (AHe age 19.3 ± 2 Ma), while uplift of the southern end of the Wooley Creek batholith (farthest from the center of the Condrey Mountain dome), which would be expected to predate that of the Slinkard pluton if Neogene structural doming centered on Condrey Mountain drove the uplift, moved to within 3 km of the surface in mid-Miocene (AHe age 15.4 ± 1.2 Ma), more recently than uplift of the Slinkard pluton to this level. In summary, thermochronometry data show that the bulk of rock uplift in the Condrey Mountain area occurred prior to Neogene time, and the post–late Miocene relative uplift of the Condrey Mountain region recorded by outward-tilted Miocene sedimentary units did not exceed ~3 km.

A regional erosion surface in the western Klamath Mountain province and Coast Ranges, the "Klamath peneplain" of Diller (1902), tilts westward and was interpreted by Aalto (2006) as evidence for low elevation of the Klamath Mountain province allowing fluvial transport across the region in late Miocene–early Pliocene time. Distribution of the peneplain in the California-Oregon Coast Ranges and in the western half of the Klamath Mountain province shows as much as 1 km of differential uplift of this surface (Irwin, 1997). The Klamath peneplain reaches its highest elevation, ~1.8 km above sea level, just east of Hoopa Valley in the southwestern Klamath Mountain province (Aalto, 2006). Sedimentologic and stratigraphic characteristics of Neogene sedimentary units deposited on the western Klamath peneplain links the peneplain surface to a record of late Miocene subsidence, followed by Pliocene–Pleistocene shoaling and emergence along the western margin of the Klamath Mountain province (Aalto, 2006). Our thermochronologic data show >7 km of exhumation in the central and southeastern Klamath Mountain province since Eocene time and are compatible with observations of the Klamath peneplain and associated onlap deposits presented by Aalto (2006).

However, early to middle Miocene Weaverville Formation sediments preserved in the Reading Creek basin record a distinctly different topographic and tectonic history in the southeastern Klamath Mountain province than that described by Aalto (2006) for the western margin of the province. The AHe age of 25.9 ± 2.9 Ma for a cobble collected from the Weaverville Formation at Reading Creek shows that the cooling age of this recycled clast is very close to that of the closest plutons currently exposed, the Shasta Bally batholith, 24.2 ± 1.9 Ma, 25.8 ± 0.9 Ma in the La Grange fault hanging wall, and the Monument Peak pluton, 22.7 ± 0.9 Ma, in the footwall (Piotraschke, 2012). This age match suggests that source rocks for Weaverville Formation conglomerate were exhumed at roughly the same time as were rocks exposed in this area today. Together, these dates imply that rapid uplift, erosion, and local deposition of recently eroded sediments occurred concurrently with, and accompanying displacement on, the La Grange fault. Fossil pollen from lacustrine sediments in the Weaverville Formation at Reading Creek includes species from montane coniferous forest, mixed evergreen-deciduous forest, and swamp forest (Barnett, 1989) and paints a picture of moderate topographic relief rather than low-relief peneplain in the southeastern Klamath Mountain province at the time of Weaverville Formation deposition. In addition, the low vitrinite reflectance of lignite from Weaverville Formation sediments at Reading Creek indicates that this area has not experienced substantial subsidence or burial since deposition of the Weaverville Formation in early middle Miocene time (Piotraschke, 2012). Therefore, there is no evidence that the southeasternmost Klamath Mountain province was reduced to a low-relief erosion surface (i.e., Klamath peneplain) in late Miocene–early Pliocene time.

Implications for Cenozoic Tectonics of the Cascadia Margin

A look northward to the Oregon Coast Ranges reveals a complex mid-Tertiary tectonic history that is recorded in the accreted Siletz terrane, and that illuminates mid-Tertiary tectonism in the Klamath Mountain province. A comprehensive geologic history of Siletzia, a large early Cenozoic igneous province in the Coast Ranges of Oregon and Washington, by Wells et al. (2014) provides a detailed chronology of Cenozoic tectonic events in the Oregon Coast Range immediately north of the Klamath Mountain province and offers a reference frame for kinematics and timing of tectonic events in the Klamath Mountain province.

The initiation of widespread uplift and exhumation of eastern Klamath Mountain province basement rocks, recorded by early Eocene AFT ages (56–48 Ma) for many plutons (the Russian Peak, Craggy Peak, Sugar Pine, and Monument Peak plutons, the Mule Mountain stock, and the unknown plutonic source of a cobble collected from the Weaverville Formation), coincided with accretion of Siletzia and with subsequent thrust faulting and folding within Siletzia reported by Wells et al. (2014). Both the spread of thermochronologic ages for samples within individual plutons and the uncertainty regarding time of initiation of Siletzia accretion preclude a simple, unambiguous correlation between Siletzia accretion and eastern Klamath Mountain province uplift, although Siletzia accretion and uplift/cooling of eastern Klamath Mountain province basement rocks were certainly occurring simultaneously.

However, both kinematics and timing link the late Eocene margin-parallel extension event in Siletzia (Tillamook magmatic episode) to north-south–directed extensional faulting in the Klamath Mountain province (La Grange fault). Sequential late Eocene north-to-south uplift of La Grange fault footwall rocks, reported previously by Batt et al. (2010b), is supported by our new late Eocene (AHe) cooling ages for plutons in the northern and central La Grange fault footwall (Russian Peak and Caribou Mountain plutons), coupled with late Eocene AFT ages (and Miocene AHe ages) in plutons at the southern end of the footwall (Canyon Creek and Granite Peak plutons).

The spatial and temporal correspondence between the accretion and subsequent deformation of the Siletzia terrane and the detachment-fault–driven exhumation of the central and eastern

Klamath terrane plutons motivates us to seek an explanation for the unroofing of the Klamaths in processes associated with the emplacement of Siletzia and the subsequent reestablishment of subduction outboard of the accreted terrane. Here, we briefly explore three possible plate-tectonic–scale processes that may have played an important role in driving the mid-Tertiary tectonic exhumation of the Klamath Mountain province: (1) Following the arguments of Wells et al. (2014), extension both in Siletzia and in the adjacent Klamath Mountain province may have been associated with interaction with the Yellowstone hotspot as western North America moved over the mantle plume; (2) margin-parallel extension may have been driven by mantle flow associated with the emplacement of the Siletzia terrane and the outboard migration of the subduction system through a process described by Moresi et al. (2014); and/or (3) margin-parallel extension in the Klamath Mountain province may have occurred in response to northward (orogeny-parallel) displacement of Siletzia as it was pushed by the northern edge of the obliquely subducting Farallon slab.

In the first scenario, during late Eocene time (ca. 42–34 Ma), the western margin of North America and the recently accreted Siletz terrane overrode the Yellowstone hotspot, as seen in margin-parallel extension, the emplacement of dike swarms, and volcanism in the central Oregon Coast Ranges (Wells et al., 2014). This extension of the Siletz terrane and additional evidence of rotation and northward migration of these recently emplaced volcanic rocks could also have provided the driver and created space to allow the mid-Tertiary margin-parallel extension and unroofing in the Klamath Mountain province. However, Liu and Stegman (2012) argued that the source of the Yellowstone volcanics first interacted with North America through a mid-Miocene rupture or tear in the Farallon slab, providing the source for the Steens Mountain volcanics in eastern Oregon, a significantly younger event than the Klamath Mountain province extension. How to reconcile the role of the Yellowstone hotspot in these two distinct (in time and location) volcanic events is not clear.

The second scenario is based on an example of margin-parallel extension that accompanied terrane accretion at a different subduction zone. Moresi et al. (2014) recently argued that, associated with the accretion of a ribbon continent (in their case, the VanDieland microcontinent in southeastern Australia), a flow regime within the upper mantle drove orogeny-parallel extension as the subduction zone propagated outboard of the newly accreted terrane. This pattern is recorded both by extension adjacent to the accreted terrane and by emplacement of relatively undeformed materials in the forearc of the reestablished subduction zone. If this scenario is applicable to Siletzia–Klamath Mountain province evolution (Fig. 6A), then the extension associated with terrane accretion (Siletzia) is manifest as the unroofing of the Klamath Mountain province accompanying extension centered on the La Grange fault, and emplacement of Coast Ranges units west of the Klamath Mountain province. In the models of Moresi et al. (2014), this extension occurred over 10–20 m.y., consistent with the time span of Klamath Mountain province unroofing.

In the third scenario, with the emplacement/accretion of Siletzia, subduction ceased inboard of the accreted terrane and reestablished itself outboard (e.g., Schmandt and Humphreys, 2011), and the slightly oblique convergence promoted extensional deformation south of the newly accreted terrane, in the Klamath Mountain province. The westward jump of subduction following accretion of Siletzia was accompanied by tearing of the Farallon slab at the southern margin of Siletzia (approximately the northern margin of the Klamath Mountain province). However, south and north of the newly accreted region, Farallon subduction likely continued unimpeded, and the subducting lithosphere north and south of Siletzia maintained its pre-accretion path, while a new slab developed outboard of Siletzia (Fig. 6B). Since Farallon subduction was slightly oblique to the North American margin, there was a northward component to the northern edge of the Farallon slab that abutted the southern margin of Siletzia. We propose that these kinematics could have driven both northward motion of Siletzia and northward motion of the adjacent Klamath Mountain province, essentially pulling the lower plate of the Klamath Mountain province northward from beneath North America. This mechanism is consistent with the long duration and relatively slow rates of extension within the Klamath Mountain province.

All of these mechanisms produce displacements of appropriate orientation and duration within the Klamath Mountain province. Whether they could work in concert or independently is unclear. Both the Moresi et al. (2014) mechanism and the slab-edge–driving mechanism we have introduced represent end members of the processes by which the subduction system is reestablished outboard of the accreted terrane. They are distinguished by whether the subduction is reestablished by the initiation of a new slab outboard of Siletzia or by the systematic northward emplacement of the ongoing Farallon subduction to the south. The role of the Yellowstone hotspot in this adds an additional complication. The position and timing of its interaction with the margin of North America may have been coincident with Klamath Mountain province exhumation, but specifically how it would drive the northward motion is not clear.

Our new data in concert with previous studies indicate that while Neogene uplift of the western margin of the Klamath Mountain province was initiated in the last several million years, as recorded by the west-tilted Klamath peneplain and overlying late Miocene and younger deposits (Aalto, 2006), the topographic relief in the southeastern Klamath Mountain province is largely a tectonic feature that developed in Oligocene–Miocene time. We argue that the formation of the Klamath massif as a persistent topographically high feature was driven by western North American plate tectonics—tectonics associated with a period of rapid and ephemeral change in subduction behavior in the region caused by the docking of an oceanic terrane (Siletzia). Key factors to linking uplift and exhumation in the southeastern Klamath Mountain province to larger-scale plate tectonics are (1) availability of a detailed geologic history for the Siletz terrane in the Oregon Coast Ranges (Wells et al., 2014), (2) timing constraints provided by low-temperature thermochronology of exhumed Klamath Mountain province plutons (Batt et al., 2010a, 2010b; Piotraschke, 2012; this study), and (3) the record of extensive, long-term brittle faulting on a regional detachment fault (Cashman and Elder, 2002; Cashman and Cashman, 2006).

The argument that the significant margin-parallel extension recorded in the exhumation of the southeastern Klamath Mountain province was driven by Farallon–North America (Siletzia) interactions demonstrates the potential for ephemeral plate-boundary configurations to produce significant tectonic remnants. In this case, without a good understanding of the timing and nature of the exhumation, the strain history recorded by faulting, and the overall plate-tectonic behavior of the plate margin, the mechanism driving extension would remain obscure.

Our initial question of whether the distinctive seismologic characteristics of the southernmost Cascadia subduction zone margin reflect the geologic character of the forearc (e.g., crust of the Klamath Mountain province) cannot be answered directly, but evidence from the central Cascadia subduction zone (latitude 43°N–46°N) suggests that rock properties within the upper plate may influence the mode of slip on the subduction zone. Global positioning system (GPS) time-series data, tide gauge records, and leveling studies in central Cascadia record lower uplift rates in this region than elsewhere along the subduction zone (Schmalzle et al., 2014), while paleoseismic records show smaller coseismic

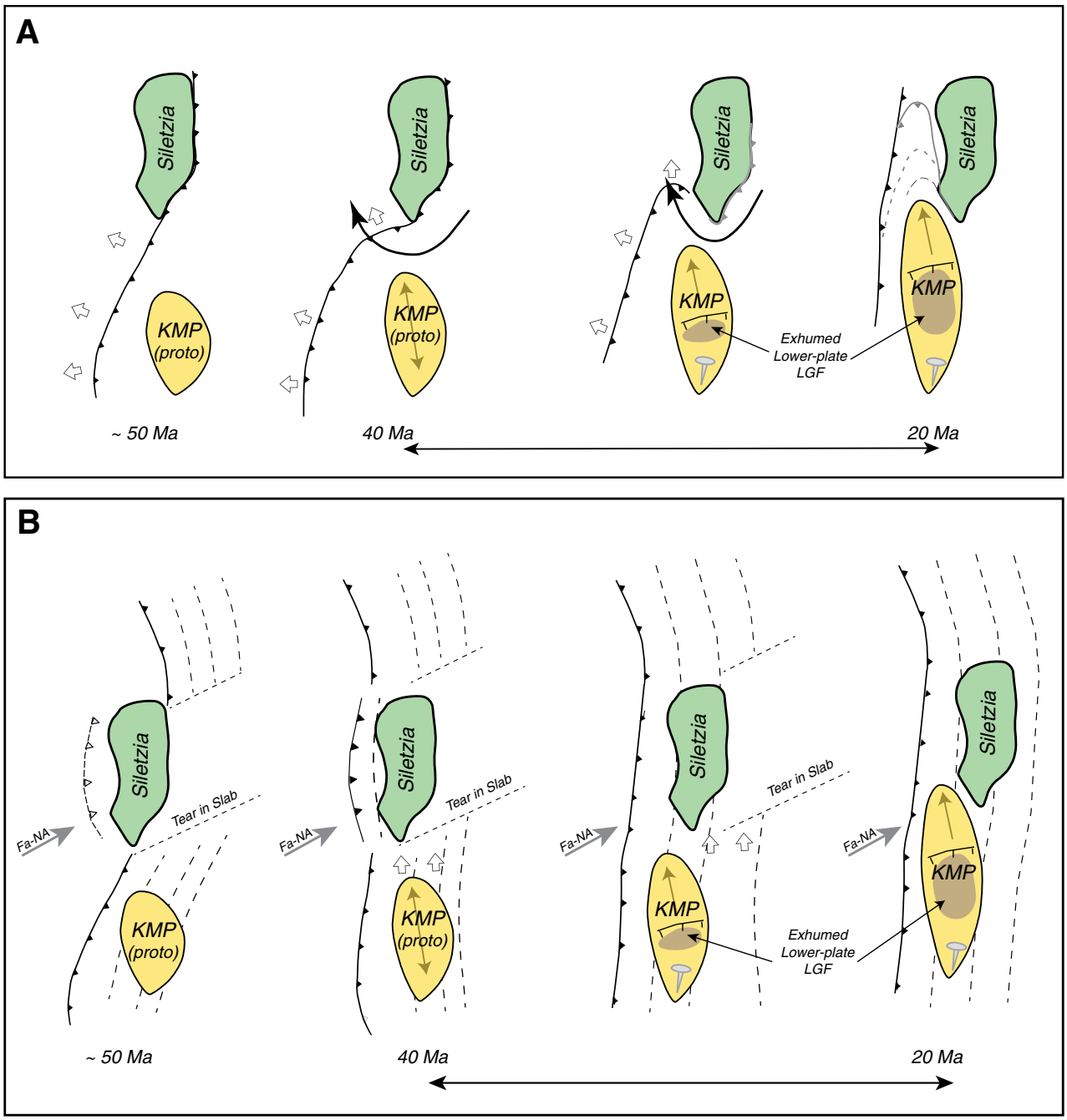

Figure 6. Schematic views of possible models of drivers for Klamath Mountain province (KMP) evolution with emplacement of Siletz terrane. (A) Moresi et al. (2014) model of consequences of ribbon-continent accretion applied to Cascadia margin and Siletzia. As a result of the emplaced continental terrane choking the subduction zone, mantle flow (shown schematically by arrows in second and third panels) drives the development of a new subduction system outboard of the accreted terrane, producing substantial extension south of the accreted terrane. In applying this to Siletzia and Klamath Mountain province, we assume that extension may be distributed initially, but once the La Grange fault (LGF) develops, extension localizes to that detachment system, and the southern end of the Klamath Mountain province is anchored to North America (shown by pin). Open arrows show migration of the trench; gray lines in 20 Ma panel show evolution of the trench as it migrates around Siletzia. Time evolution is approximate but consistent with timing from Moresi et al. (2014). (B) Proposed model from this study, invoking the northern edge of the Farallon (Fa) slab as a driver for north-south extension. At ca. 50 Ma, Siletzia docks and sutures to adjacent North America (NA), leading to slab tears within the Farallon slab north and south of Siletzia to accommodate the abrupt change in the margin. Slightly oblique convergence of the Farallon slab with respect to North America (e.g., Stock and Molnar, 1988) leads to a small northward component (shown by open arrows) to the relative plate motion, allowing the northern edge of the subducted Farallon slab to drive Siletzia and adjacent North America northward, providing both the driving mechanism and the space to accommodate extension in the Klamath Mountain province. By ca. 20 Ma, Farallon subduction is fully reestablished outboard of Siletzia, removing this driver for northward extension. Dashed lines show schematic depth contours of the subduction Benioff zone, which reestablishes beneath Siletzia by ca. 20 Ma. As in the model above, the southern Klamath Mountain province is assumed to be anchored to North America by the latter stages of the extension, leading to localized extension within the Klamath Mountain province.

subsidence during great earthquakes in the central Oregon part of the subduction zone than in neighboring parts of Cascadia (e.g., Wang et al., 2013). Schmalzle et al. (2014) suggested that the megathrust beneath central Oregon may be partially creeping, perhaps due to elevated pore-fluid pressure beneath the thick, impermeable basalt of the accreted Siletz terrane. In contrast to Siletzia and the central Oregon Coast Ranges, the Klamath Mountain province has heterogeneous rock types, a record of substantial mid-Tertiary extensional strain, and a differential local uplift history. Further geodetic and paleoseismic study of the Klamath Mountain province–southernmost Cascadia subduction zone region could help to resolve the question of the role of upper-plate structure in active seismicity in this area.

APPENDIX

(U-Th)/He Dating Analytical Procedures

For (U-Th)/He analysis, apatite crystals of similar size and shape were inspected and handpicked under a high-power optical microscope (at 50×, 200×, and 1200× magnifications, respectively) following the standard selection criteria (Farley, 2002; Brown et al., 2013). Only complete, euhedral crystals with both terminations preserved were selected in order to minimize uncertainty arising from surface and volume calculations required for alpha ejection correction (Farley et al., 1996) and to minimize possible dispersion of (U-Th)/He ages (Brown et al., 2013). Selected crystals were photographed, measured for dimensions, and loaded in Pt tubes. Single apatite crystals were degassed at ~960 °C under ultrahigh vacuum using laser heating and analyzed for ^{4}He by isotope dilution on extraction systems designed by Patterson Instruments, Ltd., with a Pfeiffer Prisma QMS-200 mass spectrometer in the Thermochronology Laboratory of the University of Waikato. Details of analytical protocols of He measurement can be found in Danišík et al. (2012a, 2012b). Following He measurements, the apatite grains were spiked with ^{235}U and ^{230}Th isotopes and dissolved in nitric acid following the protocols of Evans et al. (2005). The solutions were analyzed by isotope dilution for U and Th on a PerkinElmer SCIEX ELAN DRC II inductively coupled plasma–mass spectrometer. Total analytical uncertainty (TAU) was calculated as the square root of the sum of the squares of weighted uncertainties on U, Th, and He measurements. The raw (U-Th)/He ages were corrected for alpha ejection (Ft correction) after Farley et al. (1996). A value of 5% was adopted as the uncertainty on the Ft correction and was used to calculate errors for the corrected (U-Th)/He ages. Single-crystal (U-Th)/He ages with associated analytical uncertainties were used to calculate the geometric mean as a representative number for each sample set using RadialPlotter (Table 2; Vermeesch, 2009). Replicate analyses of Durango apatite (n = 38) measured over the period of this study as an internal standard yielded mean (U-Th)/He ages of 30.8 ± 1.4 Ma, which is in excellent agreement with the Durango (U-Th)/He age of 31.02 ± 1.01 Ma (McDowell et al., 2005).

Fission-Track Analysis Analytical Procedures

Sample preparation and experimental methods used in this study follow those reported by Green (1985) and Gleadow et al. (1986), as adopted in the University of Waikato Fission Track Laboratory (Kamp et al., 1989, 1992). Apatite concentrates were separated from 1 kg samples of plutons using standard crushing, magnetic, and heavy liquid techniques. The external detector method (Gleadow, 1981) was used exclusively in this study. Apatite mounts were etched in 5 M HNO_3 at 20 °C for 20 s and irradiated in the ANSTO (Australian Nuclear Science and Technology Organisation) reactor at Lucas Heights, Sydney, Australia, with nominal fluences of 1×10^{16} n/cm^2 for apatite. The fission-track ages were determined using the zeta calibration method (Green, 1985; Hurford and Green, 1982) and calculated as central ages (Galbraith and Green, 1990) as $P(\chi^2)$ values are much greater than 5% (Table 1). Confined track lengths in apatite were measured using a digitizing tablet connected to a computer, superimposed on the microscope field of view via a projection tube. Tracks were measured using the recommendations of Laslett et al. (1982).

ACKNOWLEDGMENTS

We thank Kyle French for assistance in the field, and Tim White for vitrinite reflectance analyses and help with interpretation of those data. We are grateful to Don Elder, Gene Humphries, Harvey Kelsey, Ken Creager, and Ray Wells for helpful discussions, and to Pat Cashman, Art Snoke, and two anonymous reviewers for insightful and productive critiques of an earlier version of the paper. We gratefully acknowledge support from Pennsylvania State University, Department of Geosciences' Fund for Excellence in Lithospheric Geodynamics and the Krynine fund for support for Piotraschke for travel and geochronology analyses.

REFERENCES CITED

Aalto, K.R., 2006, The Klamath peneplain: A review of J.S. Diller's classic erosion surface, *in* Soke, A.W., and Barnes, C.G., eds., Geological Studies in the Klamath Mountains Province, California and Oregon: A Volume in Honor of William P. Irwin: Geological Society of America Special Paper 410, p. 451–463, doi:10.1130/2006.2410(22).

Albers, P.J., Kistler, R.W., and Kwak, L., 1981, The Mule Mountain stock, an early Middle Devonian pluton in northern California: Isochron-West, v. 31, p. 17.

Allen, C.M., and Barnes, C.G., 2006, Ages and some cryptic sources of Mesozoic plutonic rocks in the Klamath Mountains, California and Oregon, *in* Snoke, A.W., and Barnes, C.G., eds., Geological Studies in the Klamath Mountains Province, California and Oregon: A Volume in Honor of William P. Irwin: Geological Society of America Special Paper 410, p. 223–245, doi:10.1130/2006.2410(11).

Barnes, C.G., Allen, C.M., and Saleeby, J.B., 1986, Open- and closed-system characteristics of a tilted plutonic system, Klamath Mountains, California: Journal of Geophysical Research, v. 91, p. 6073–6090, doi:10.1029/JB091iB06p06073.

Barnes, C.G., Barnes, M., and Kistler, R.W., 1992, Petrology of the Caribou Mountain pluton, Klamath Mountains, California: Journal of Petrology, v. 33, p. 95–124, doi:10.1093/petrology/33.1.95.

Barnes, C.G., Petersen, S.W., Kistler, R.W., Murray, R., and Kays, M.A., 1996, Source and tectonic implications of tonalite-trondhjemite magmatism in the Klamath Mountains: Contributions to Mineralogy and Petrology, v. 123, p. 40–60, doi:10.1007/s004100050142.

Barnett, J., 1989, Palynology and paleoecology of the Tertiary Weaverville Formation, northwestern California, U.S.A.: Palynology, v. 13, p. 195–246, doi:10.1080/01916122.1989.9989361.

Batt, G.E., Harper, G.D., Heizler, M., and Roden-Tice, M., 2010a, Cretaceous sedimentary blanketing and tectonic rejuvenation in the western Klamath Mountains: Insights from thermochronology: Central European Journal of Geosciences, v. 2, p. 138–151, doi:10.2478/v10085-009-0041-4.

Batt, G.E., Cashman, S.M., Garver, J., and Bigelow, J.J., 2010b, Thermotectonic evidence for two-stage extension on the Trinity detachment surface, Eastern Klamath Mountains, California: American Journal of Science, v. 310, p. 261–281, doi:10.2475/04.2010.02.

Beaudoin, B.C., Godfrey, N.J., Klemperer, S.L., Lendl, C., Trehu, A.M., Henstock, T.J., Levander, A., Holl, J.E., Meltzer, A.S., and Mooney, W.D., 1996, Transition from slab to slabless: Results from the 1993 Mendocino triple junction seismic experiment: Geology, v. 24, p. 195–199, doi:10.1130/0091-7613(1996)024<0195:TFSTSR>2.3.CO;2.

Boyarko, D., and Brudzinski, M., 2010, Spatial and temporal patterns of nonvolcanic tremor along the southern Cascadia subduction zone: Journal of Geophysical Research, v. 115, no. B8, p. B00A22, doi:10.1029/2008JB006064.

Brichau, S., Ring, U., Ketcham, R.A., Carter, A., Stockli, D., and Brunel, M., 2006, Constraining the long-term evolution of the slip rate for a major extensional fault system in the central Aegean, Greece, using thermochronology: Earth and Planetary Science Letters, v. 241, p. 293–306, doi:10.1016/j.epsl.2005.09.065.

Brown, R.W., Beucher, R., Roper, S., Persano, C., Stuart, F., and Fitzgerald, P., 2013, Natural age dispersion arising from the analysis of broken crystals: Part I. Theoretical basis and implications for the apatite (U-Th)/He thermochronometer: Geochimica et Cosmochimica Acta, v. 122, p. 478–497, doi:10.1016/j.gca.2013.05.041.

Brudzinski and Allen, 2007, Segmentation and episodic tremor and slip all along Cascadia: Geology, v. 35, p. 907–910, doi:10.1130/G23740A.1.

Carter, T.J., Kohn, B.P., Foster, D.A., Gleadow, A.J.W., and Woodhead, J.D., 2006, Late-stage evolution of the Chemehuevi and Sacramento detachment faults from apatite (U-Th)/He thermochronometry—Evidence for mid-Miocene accelerated slip: Geological Society of America Bulletin, v. 118, p. 689–709, doi:10.1130/B25736.1.

Cashman, S.M., and Cashman, K.V., 2006, Cataclastic textures in La Grange fault rocks, Klamath Mountains, California, *in* Snoke, A.W., and Barnes, C.G., eds., Geological Studies in the Klamath Mountains Province, California and Oregon: A Volume in Honor of William P. Irwin: Geological Society of America Special Paper 410, p. 433–450, doi:10.1130/2006.2410(21).

Cashman, S.M., and Elder, D.R., 2002, Post-Nevadan detachment faulting in the Klamath Mountains, California: Geological Society of America Bulletin, v. 114, p. 1520–1534, doi:10.1130/0016-7606(2002)114<1520:PNDFIT>2.0.CO;2.

Coint, N., Barnes, C.G., Yoshinobu, A.S., Chamberlain, K.R., and Barnes, M.A., 2013, Batch-wise assembly and zoning of a tilted calc-alkaline batholith: Field relations, timing, and compositional variation: Geosphere, v. 9, p. 1729–1746, doi:10.1130/GES00930.1.

Coney, P.J., Jones, D.L., and Monger, J.W.H., 1980, Cordilleran suspect terranes: Nature, v. 288, p. 329–333, doi:10.1038/288329a0.

Cotkin, S.J., and Medaris, L.G., 1993, Evaluation of the crystallization conditions for the calcalkaline Russian Peak intrusive complex, Klamath Mountains, northern California: Journal of Petrology, v. 34, p. 543–571, doi:10.1093/petrology/34.3.543.

Danišík, M., Kuhlemann, J., Dunkl, I., Székely, B., Evans, N.J., and Frisch, W., 2012a, Survival of ancient landforms in a collisional setting as revealed by combined fission track and (U-Th)/He thermochronometry: A case study from Corsica (France): The Journal of Geology, v. 120, no. 2, p. 155–173, doi:10.1086/663873.

Danišík, M., Štěpančíková, P., and Evans, N.J., 2012b, Constraining long-term denudation and faulting history in intraplate regions by multisystem thermochronology: An example of the Sudetic marginal fault (Bohemian Massif, central Europe): Tectonics, v. 31, p. TC2003, doi:10.1029/2011TC003012.

Davis, G.A., 1963, Structure and mode of emplacement of Caribou Mountain pluton, Klamath Mountains, California: Geological Society of America Bulletin, v. 74, p. 331–348, doi:10.1130/0016-7606(1963)74[331:SAMOEO]2.0.CO;2.

Diller, J.S., 1902, Topographic Development of the Klamath Mountains: U.S. Geological Survey Bulletin 196, 69 p.

Dodson, M.H., 1973, Closure temperature in cooling geochronological and petrological systems: Contributions to Mineralogy and Petrology, v. 40, p. 259–274, doi:10.1007/BF00373790.

DuRoss, C.B., Blakely, R.J., and Wells, R.E., 2002, Geologic cross sections through the Roseburg 30′ Â~ 60′ quadrangle, Oregon: New constraints from potential field modeling: Geological Society of America Abstracts with Programs, v. 34, no. 5, p. 32.

Ernst, W.G., Snow, C.A., and Scherer, H.H., 2008, Contrasting early and late Mesozoic petrotectonic evolution of northern California: Geological Society of America Bulletin, v. 120, p. 179–194, doi:10.1130/B26173.1.

Evans, N.J., Byrne, J.P., Keegan, J.T., and Dotter, L.E., 2005, Determination of uranium and thorium in zircon, apatite, and fluorite: Application to laser (U-Th)/He thermochronology: Journal of Analytical Chemistry, v. 60, no. 12, p. 1159–1165, doi:10.1007/s10809-005-0260-1.

Farley, K.A., 2002, (U-Th)/He dating: Techniques, calibrations, and applications: Reviews in Mineralogy and Geochemistry, v. 47, p. 819–844, doi:10.2138/rmg.2002.47.18.

Farley, K.A., Wolf, R.A., and Silver, L.T., 1996, The effect of long alpha stopping distances on (U-Th)/He ages: Geochimica et Cosmochimica Acta, v. 60, no. 21, p. 4223–4229, doi:10.1016/S0016-7037(96)00193-7.

Frey, M., de Capitani, C., and Liou, J.G., 1991, A new petrogenetic grid for metabasites: Journal of Metamorphic Geology, v. 9, p. 497–509, doi:10.1111/j.1525-1314.1991.tb00542.x.

Furlong, K.P., and Govers, R., 1999, Ephemeral crustal thickening at a triple junction: The Mendocino crustal conveyor: Geology, v. 27, p. 127–130, doi:10.1130/0091-7613(1999)027<0127:ECTAAT>2.3.CO;2.

Furlong, K.P., and Schwartz, S.Y., 2004, Influence of the Mendocino triple junction on the tectonics of coastal California: Annual Review of Earth and Planetary Sciences, v. 32, p. 403–433, doi:10.1146/annurev.earth.32.101802.120252.

Furlong, K.P., Lock, J., Guzofski, C., Whitlock, J., and Benz, H., 2003, The Mendocino crustal conveyor: Making and breaking the California crust: International Geology Review, v. 45, p. 767–779, doi:10.2747/0020-6814.45.9.767.

Galbraith, R.F., 1981, On statistical models for fission track counts: Mathematical Geology, v. 13, p. 471–478.

Galbraith, R.F., and Green, P.F., 1990, Estimating the component ages in a finite mixture: International Journal of Radiation Applications and Instrumentation, Part D, Nuclear Tracks and Radiation Measurements, v. 17, no. 3, p. 197–206, doi:10.1016/1359-0189(90)90035-V.

Gleadow, A.J.W., 1981, Fission track dating methods: What are the real alternatives?: Nuclear Tracks and Radiation Measurements, v. 5, p. 15–25.

Gleadow, A.J.W., Duddy, I.R., Green, P.F., and Hegarty, K.A., 1986, Fission track lengths in the apatite annealing zone and the interpretation of mixed ages: Earth and Planetary Science Letters, v. 78, no. 2–3, p. 245–254, doi:10.1016/0012-821X(86)90065-8.

Gomberg, J., and the Cascadia 2007 and Beyond Working Group, 2010, Slow-slip phenomena in Cascadia from 2007 and beyond: A review: Geological Society of America Bulletin, v. 122, p. 963–978, doi:10.1130/B30287.1.

Goodge, J.W., 1989, Evolving early Mesozoic convergent margin deformation, central Klamath Mountains, northern California: Tectonics, v. 8, p. 845–864, doi:10.1029/TC008i004p00845.

Green, P.F., 1985, Comparison of zeta calibration baseline for fission track dating of apatite, zircon and sphere: Chemical Geology, v. 58, p. 1–22, doi:10.1016/0168-9622(85)90023-5.

Hacker, B.R., Donato, M.M., Barnes, C.G., McWilliams, M.O., and Ernst, W.G., 1995, Timescales of orogeny: Jurassic construction of the Klamath Mountains: Tectonics, v. 14, p. 677–703, doi:10.1029/94TC02454.

Hotz, P.E., 1971, Plutonic Rocks of the Klamath Mountains, California and Oregon: U.S. Geological Survey Professional Paper 684-B, 20 p.

Hurford, A.J., and Green, P.F., 1982, A guide to fission track dating calibration: Earth and Planetary Science Letters, v. 59, p. 343–354, doi:10.1016/0012-821X(82)90136-4.

Irwin, W.P., 1960, Geologic Reconnaissance of the Northern Coast Ranges and Klamath Mountains, California, with a Summary of the Mineral Resources: California Division of Mines and Geology Bulletin 179, 80 p.

Irwin, W.P., 1972, Terranes of the Western Paleozoic and Triassic Belt in the Southern Klamath Mountains, California: U.S. Geological Survey Professional Paper 800-C, p. C103–C111.

Irwin, W.P., 1981, Tectonic accretion of the Klamath Mountains, *in* Ernst, W.G., ed., The Geotectonic Development of California—Rubey Volume I: Englewood Cliffs, New Jersey, Prentice-Hall, p. 29–49.

Irwin, W.P., 1985, Age and tectonics of plutonic belts in accreted terranes of the Klamath Mountains, California and Oregon, *in* Howell, D.G., ed., Tectonostratigraphic Terranes of the Circum-Pacific Region: Circum-Pacific Council for Energy and Mineral Resources Earth Science Series 1, p. 187–199.

Irwin, W.P., 1994, Geologic Map of the Klamath Mountains, California and Oregon: U.S. Geological Survey Miscellaneous Investigations Series I-2148, scale 1:500,000, 2 sheets.

Irwin, W.P., 1997, Preliminary Map of Selected post-Nevadan Geologic Features of the Klamath Mountains and Adjacent Areas, California and Oregon: U.S. Geological Survey Open-File Report 97-465, 29 p.

Irwin, W.P., and Lipman, P.W., 1962, A Regional Ultramafic Sheet in Eastern Klamath Mountains, California: U.S. Geological Survey Professional Paper, v. 450-C, p. C18–C21.

Irwin, W.P., and Wooden, J.L., 1989, Plutons and accretionary episodes of the Klamath Mountains, California and Oregon: U.S. Geological Survey Open-File Report 99-374, 1 sheet.

Jachens, R.C., Barnes, C.G., and Donato, M.M., 1986, Subsurface configuration of the Orleans fault: Implications for deformation in the western Klamath Mountains, California: Geological Society of America Bulletin, v. 97, no. 4, p. 388–395, doi:10.1130/0016-7606(1986)97<388:SCOTOF>2.0.CO;2.

Kamp, P.J.J., Green, P.F., and White, S.H., 1989, Fission track analysis reveals character of collisional tectonics in New Zealand: Tectonics, v. 8, p. 169–195, doi:10.1029/TC008i002p00169.

Kamp, P.J.J., Green, P.F., and Tippett, J.M., 1992, Tectonic architecture of the mountain front–foreland basin transition, South Island, New Zealand, assessed by fission track analysis: Tectonics, v. 11, p. 98–113, doi:10.1029/91TC02362.

Kelsey, H.M., Engebretson, D.C., Mitchell, C.E., and Ticknor, R.L., 1994, Topographic form of the Coast Ranges of the Cascadia margin in relation to coastal uplift rates and plate subduction: Journal of Geophysical Research, v. 99, p. 12,245–12,255, doi:10.1029/93JB03236.

Laslett, G.M., Kendall, W.S., Gleadow, A.J.W., and Duddy, I.R., 1982, Bias in the measurement of fission track length distributions: Nuclear Tracks and Radiation Measurements, v. 6, p. 79–85, doi:10.1016/0735-245X(82)90031-X.

Liu, K., Levander, A., Zhai, Y., Porrit, R., and Allen, R.M., 2012, Asthenospheric flow and lithospheric evolution near the Mendocino triple junction: Earth and Planetary Science Letters, v. 323–324, p. 60–71, doi:10.1016/j.epsl.2012.01.020.

Liu, L., and Stegman, D.R., 2012, Origin of Columbia River flood basalt controlled by propagating rupture of the Farallon slab: Nature, v. 482, p. 386–389, doi:1038/nature10749.

Lock, J., Kelsey, H., Furlong, K., and Woolace, A., 2006, Late Neogene and Quaternary landscape evolution of the northern California Coast Ranges: Evidence for Mendocino triple junction tectonics: Geological Society of America Bulletin, v. 118, p. 1232–1246, doi:10.1130/B25885.1.

MacDonald, D.F., 1910, The Weaverville–Trinity Center Gold Gravels, Trinity County, California: U.S. Geological Survey Bulletin 430, p. 48–58.

McDowell, F.W., McIntosh, W.C., and Farley, K.A., 2005, A precise $^{40}Ar/^{39}Ar$ reference age for the Durango apatite (U-Th)/He and fission track dating standard: Chemical Geology, v. 214, p. 249–263, doi:10.1016/j.chemgeo.2004.10.002.

McLaughlin, R.J., Ellen, S.D., Blake, M.C., Jr., Jayco, A.S., Irwin, W.P., Aalto, K.R., Carver, G.A., and Clarke, S.H., Jr., 2000, Geology of the Cape Mendocino, Eureka, Garberville, and Southwestern Part of the Hayfork 30 × 60 Minute Quadrangles and Adjacent Offshore Area, Northern California: U.S. Geological Survey Miscellaneous Field Studies Map MF-2336, scale 1:100,000.

Moresi, L., Betts, P.G., Miller, M.S., and Cayley, R.A., 2014, Dynamics of continental accretion: Nature, v. 508, p. 245–248, doi:10.1038/nature13033.

Mortimer, N., and Coleman, R.G., 1985, A Neogene structural dome in the Klamath Mountains, California: Geology, v. 13, p. 253–256, doi:10.1130/0091-7613(1985)13<253:ANSDIT>2.0.CO;2.

Phillips, P.A., and Aalto, K.R., 1989, The Weaverville Formation: Implications for tectonically-controlled basin development in the central Klamath Mountains, *in* Coburn, I., and Minch, J., eds., Conglomerates in Basin Analysis: Pacific Section, Society of Economic Paleontologists and Mineralogists, Book 62, p. 81–98.

Piotraschke, R., 2012, Thermal and Geologic Constraints on the Cretaceous-to-Neogene Tectonic Development of the Klamath Mountains, Northern California [M.S. thesis]: University Park, Pennsylvania State University, 102 p.

Schmalzle, G.M., McCaffrey, R., and Creager, K.C., 2014, Central Cascadia subduction zone creep: Geochemistry Geophysics Geosystems, v. 15, p. 1515–1532, doi:10.1002/2013GC005172.

Schmandt, B., and Humphreys, E., 2011, Seismically imaged relict slab from the 55 Ma Siletzia accretion to the northwest United States: Geology, v. 39, p. 175–178, doi:10.1130/G31558.1.

Schweickert, R.A., and Irwin, W.P., 1989, Extensional faulting in southern Klamath Mountains, California: Tectonics, v. 8, p. 135–149, doi:10.1029/TC008i001p00135.

Sliter, W.V., Jones, D.L., and Throckmorton, C.K., 1984, Age and correlation of the Cretaceous Hornbrook Formation, California and Oregon, *in* Nilsen, T.H., ed., Geology of the Upper Cretaceous Hornbrook Formation, Oregon and California: Pacific Section, Society of Economic Paleontologists and Mineralogists, Book 42, p. 89–98.

Snoke, A.W., and Barnes, C.G., 2006, The development of tectonic concepts for the Klamath Mountains province, California and Oregon, *in* Snoke, A.W., and Barnes, C.G., eds., Geological Studies in the Klamath Mountains Province, California and Oregon: A Volume in Honor of William P. Irwin: Geological Society of America Special Paper 410, p. 1–29, doi:10.1130/2006.2410(01).

Stock, J., and Molnar, P., 1988, Uncertainties and implications of the Late Cretaceous and Tertiary position of North America relative to the Farallon, Kula, and Pacific plates: Tectonics, v. 7, p. 1339–1384, doi:10.1029/TC007i006p01339.

Surpless, K.D., and Beverly, E.J., 2013, Understanding a critical basinal link in Cretaceous Cordilleran paleogeography: Detailed provenance of the Hornbrook Formation, Oregon and California: Geological Society of America Bulletin, v. 125, no. 5–6, p. 709–727, doi:10.1130/B30690.1.

Szeliga, W., T.I. Melbourne, M.M. Miller, and V.M. Santillan, 2004, Southern Cascadia episodic slow earthquakes, 2004: Geophysical Research Letters, v. 31, p. L16602, doi:10.1029/2004GL020824.

Vermeesch, P., 2009, RadialPlotter: A Java application for fission track, luminescence and other radial plots: Radiation Measurements, v. 44, no. 4, p. 409–410, doi:10.1016/j.radmeas.2009.05.003.

Wagner, D.L., and Saucedo, G.J., compilers, 1987, Geologic Map of the Weed Quadrangle, California: California Division of Mines and Geology Regional Geologic Map Series Map 4A, scale 1:250,000.

Wallin, E.T., Coleman, D.S., Lindsley-Griffin, N., and Potter, A.W., 1995, Silurian plutonism in the Trinity terrane (Neoproterozoic and Ordovician), Klamath Mountains, California, USA: Tectonics, v. 14, p. 1007–1013, doi:10.1029/95TC01447.

Wang, P., Englehart, S.E., Wang, K., Hawkes, A.D., Horton, B.P., Nelson, A.R., and Witter, R.C., 2113, Heterogeneous rupture in the Great Cascadia Earthquake of 1700 inferred from coastal subsidence estimates: Journal of Geophysical Research–Solid Earth, v. 118, p. 2460–2473, doi:10.1002/jgrb.50101.

Wells, R., Jayko, A.S., Niem, A.R., Black, G., Wiley, T., Baldwin, E., Molenaar, K.M., Wheeler, K.L., DuRoss, C.B., and Givler, R.W., 2000, Geologic Map and Database of the Roseburg 30 × 60′ Quadrangle, Douglas and Coos Counties, Oregon: U.S. Geological Survey Open-File Report 00-376.

Wells, R., Bukry, D., Friedman, R., Pyle, D., Duncan, R., Haeussler, P., and Wooden, J., 2014, Geologic history of Siletzia, a large igneous province in the Oregon and Washington Coast Range: Correlation to the geomagnetic polarity time scale and implications for a long-lived Yellowstone hotspot: Geosphere, v. 10, p. 692–719, doi:10.1130/GES01018.1.

Zucca, J.J., Fuis, G.S., Milkereit, B., Mooney, W.D., and Catchings, R.D., 1986, Crustal structure of northern California: Journal of Geophysical Research, v. 91, no. B7, p. 7359–7382, doi:10.1029/JB091iB07p07359.

MANUSCRIPT RECEIVED 7 SEPTEMBER 2014
REVISED MANUSCRIPT RECEIVED 23 FEBRUARY 2015
MANUSCRIPT ACCEPTED 25 APRIL 2015

Printed in the USA